

## On the Color-Metallicity Relation of the Red Clump and the Reddening Toward the Magellanic Clouds

DAVID M. NATAF,<sup>1</sup> SANTI CASSISI,<sup>2,3</sup> LUCA CASAGRANDE,<sup>4</sup> AND ADAM G. RIESS<sup>5,1</sup>

<sup>1</sup>*Center for Astrophysical Sciences and Department of Physics and Astronomy, The Johns Hopkins University, Baltimore, MD 21218*

<sup>2</sup>*INAF-Osservatorio Astronomico d'Abruzzo, via M. Maggini, sn. I-64100 Teramo, Italy*

<sup>3</sup>*INFN-Sezione di Pisa, Largo Pontecorvo 3, I-56127 Pisa, Italy*

<sup>4</sup>*Research School of Astronomy and Astrophysics, Mount Stromlo Observatory, The Australian National University, ACT 2611, Australia*

<sup>5</sup>*Space Telescope Science Institute, 3700 San Martin Drive, Baltimore, MD 21218, USA*

### ABSTRACT

The zero point of the reddening toward the Large Magellanic Cloud (LMC) has been the subject of some dispute. Its uncertainty propagates as a systematic error for methods which measure the extragalactic distance scale through knowledge of the absolute extinction of LMC stars. In an effort to resolve this issue, we used three different methods to calibrate the most commonly used metric to predict LMC extinction, the intrinsic color of the red clump,  $(V - I)_{RC,0}$ . The first approach was to empirically calibrate the color zeropoints of the BaSTI isochrones over a wide metallicity range of  $\Delta[\text{Fe}/\text{H}] \approx 1.10$  using measurements of red clump stars in 47 Tuc, the Solar Neighborhood, and NGC 6791. From these efforts we also measure these properties of the Solar Neighborhood red clump,  $(V - I, G_{BP} - K_s, G - K_s, G_{RP} - K_s, J - K_s, H - K_s, M_I, M_{K_s})_{RC,0} = (1.02, 2.75, 2.18, 1.52, 0.64, 0.15, -0.23, -1.63)$ . The second and third methods were to compare the observed colors of the red clump to those of Cepheids and RR Lyrae in the LMC which are standardizable crayons based on their periods and metallicities. With these three methods, we estimated the intrinsic color of the red clump of the LMC to be  $(V - I)_{RC,0,LMC} = \{0.90, 0.93, 0.93\}$  respectively, and similarly using the first and third method we estimated  $(V - I)_{RC,0,SMC} = \{0.85, 0.88\}$  respectively for the Small Magellanic Cloud. We estimate the luminosities to be  $M_{I,RC,LMC} = -0.31$  and  $M_{I,RC,SMC} = -0.39$ . We show that this has important implications for recent calibrations of the tip of the red giant branch in the Magellanic Clouds used to measure  $H_0$ .

### 1. INTRODUCTION

The red clump, which is the horizontal branch of a metal-rich ( $[\text{Fe}/\text{H}] \gtrsim -1.0$ ) stellar population, is a long-lived and thus well populated evolutionary stage and predicted by stellar theory to have precise color-metallicity and luminosity-metallicity relations (Girardi & Salaris 2001; Salaris & Girardi 2002). The red clump has thus been a widely used “standard crayon” and standard candle to characterize stellar populations over a wide range of ages, for example the mapping of the chemical gradients of the Milky Way Disk (Nidever et al. 2014); mapping the reddening toward the Milky Way’s nuclear disk (Nogueras-Lara et al. 2019); the reddening variations (Nataf et al. 2016), bar morphology (Stanek et al. 1997), peanut/X-shape profile (Nataf et al. 2010; McWilliam & Zoccali 2010) and the long bar component (Wegg et al. 2015) of the Milky Way Bulge; the reddening toward the Magellanic Clouds (Haschke et al. 2011; Górski et al. 2020); the reddening

of the Tip of the Red Giant Branch (TRGB) for distance scale work Jang & Lee (2017a,b); Yuan et al. (2019), and the reddening of and distance to the Sagittarius stream (Correnti et al. 2010; Carrell et al. 2012) and the Andromeda galaxy (Stanek & Garnavich 1998; Cohen et al. 2018).

That is an impressive breadth of discovery and diagnostic power, and one which we expect may grow in the coming decade as several new observatories come online. Each of the *James Webb Space Telescope (JWST)*, the *Wide-Field Infrared Survey Telescope (WFIRST)*, the *Giant Magellan Telescope (GMT)*, the *Thirty Meter Telescope (TMT)*, and the *European Extremely Large Telescope (E-ELT)* (Gilmozzi & Spyromilio 2007) will be maximally sensitive for wavelengths with  $\lambda \gtrsim 1\mu\text{m}$ , a regime where red clump stars are intrinsically bright due to their cool ( $T_{\text{eff}} \approx 4,500\text{ K}$ ) effective temperatures. For example,  $M_{RC,K_s} \approx -1.62$  for the stellar population of the solar neighbourhood (Hawkins et al. 2017; Chan & Bovy 2019; Chen et al. 2017).

We have thus been motivated to explore a discrepancy in the assumed intrinsic red clump optical color  $(V - I)_{RC,0}$  in the recent literature. The assumption directly affects the red-

dening toward the Large Magellanic Cloud (LMC), for which the widely used reddening map of [Haschke et al. \(2011\)](#) had assumed  $(V - I)_{RC,0,LMC} = 0.92$ . This assumption is corroborated by other methods. For example, the reddening map of [Inno et al. \(2016\)](#), which is derived from measurements of classical Cepheids, measured a reddening toward the LMC that was 0.02 mag greater in the mean, an offset smaller than the reported errors. However, the recent investigation of [Górski et al. \(2020\)](#) derived a much bluer value, of  $(V - I)_{RC,0,LMC} = 0.838 \pm 0.034$  for the LMC.

That offset, of 0.08 mag in  $(V - I)_{RC,0,LMC}$ , is substantially larger than the reported errors of most, and indeed perhaps all, recent investigations that assume an intrinsic color for the red clump. It may be due to factors such as undiagnosed population effects in the LMC stellar population, or the red clump color-metallicity relation having a very different slope than commonly assumed. Either finding would necessitate a revision of much of the literature on stellar astrophysics, interstellar reddening, and the distance scale. It also might have a simpler explanation if the sight lines of young, Blue Supergiants used by [Górski et al. \(2020\)](#) to deredden red clump stars are dustier than those of the older, Red Giants which we consider in Section 5.

The purpose of this work is to investigate the issue of the red clump’s color-metallicity relation, and to derive robust zeropoints for the Red Clump for use in the LMC and the Small Magellanic Cloud (SMC). We first review the theoretical and empirical calibration of the red clump in Section 2. We verify the consistency of these estimates for the LMC and SMC in Section 3. In Section 4, we evaluate the consistency of the predicted value of  $(V - I)_{RC,0}$  for the LMC and SMC with calibrations from RRab stars and exquisitely measured Cepheids. We discuss our findings and present our conclusions in Sections 5 and 6.

## 2. CALIBRATION OF THE RED CLUMP

In this Section we will employ a hybrid empirical and theoretical approach to predict the color and magnitude of the red clumps of the Large and Small Magellanic Clouds. We will follow the approach of [Girardi & Salaris \(2001\)](#) and [Salaris & Girardi \(2002\)](#), in which the trends of red clump color and magnitude with age and metallicity are derived from stellar models, but the zero points are shifted to agree with the best available empirical data.

The red clumps of the globular cluster 47 Tuc, of the solar neighbourhood, and of the open cluster NGC 6791 will be used to calibrate the zero points. For each of those three stellar populations, and both Magellanic Clouds, we will state both our assumed population parameters ( $[Fe/H]$ ,  $[\alpha/Fe]$ , etc), as well as other robust estimates from the literature, as the uncertainty in population parameters contributes to the uncertainty in the overall calibration.

For the chemical abundances ( $[Fe/H]$ ,  $[\alpha/Fe]$ ) we assume the parameters derived by the ASPCAP pipeline ([García Pérez et al. 2016](#)) from spectra taken for APOGEE ([Majewski et al. 2017](#)), a high-resolution ( $R \sim 22,500$ , high signal-to-noise (SNR  $\sim 100$ ) Galactic archaeology spectroscopic survey that is part of the Sloan Digital Sky Survey ([Blanton et al. 2017](#)). This survey is chosen as it has large numbers of consistent measurements of the stellar populations studied in this work. The  $[Fe/H]$  abundances are consistent with prior literature values, with a mean and standard deviation in the offset with respect to 525 “standard stars” of  $\Delta[Fe/H] = 0.04 \pm 0.10$  dex, and is largely a uniform shift, without a metallicity trend (Table 4 and Figure 3 of [Jönsson et al. 2018](#), respectively). We also verify that this is the case for the particular populations studied in this work. We use these abundances not just for the LMC and SMC, but for all stellar populations discussed in this work, to ensure a homogeneous metallicity scale.

### 2.1. Population Parameters for the Large and Small Magellanic Clouds

We assume the star-formation histories measured by [Weisz et al. \(2013\)](#). These were derived by comparing deep color-magnitude diagrams observed with *HST*, with synthetic color-magnitude diagrams created by MATCH ([Dolphin 2002](#)). The resulting mean ages for the LMC and SMC stellar populations are 6 and 5 Gyr respectively.

We use the abundances of faint red giants and bright red giants, as defined by [Nidever et al. \(2019\)](#) for the APOGEE LMC fields of LMC{4,5,6,8,9,13,14} and SMC fields of SMC{3,4,5}. We exclude stars with  $\log g \geq 2$ , and stars with  $[Fe/H] \leq -1.1$  as likely not contributing to the red clump. This yields a sample of 882 red giants in the LMC, and 310 red giants in the SMC. The resulting mean values of ( $\langle [Fe/H] \rangle$ ,  $\langle [\alpha/Fe] \rangle$ ) are  $(-0.64, +0.03)$  and  $(-0.88, -0.02)$  for the LMC and SMC respectively. A cut at  $[Fe/H] \leq -1.5$  would shift the effective mean metallicities by 0.04 and 0.08 dex for the LMC and SMC respectively.

These are consistent with other literature values. From the work of [Van der Swaelmen et al. \(2013\)](#), we find that the mean abundance of 148 LMC bar and disk stars satisfying  $[M/H] \geq -1.1$  is  $\langle [M/H] \rangle = -0.64$ . Similarly, from the work of [Parisi et al. \(2016\)](#) we find an abundance of  $\langle [Fe/H] \rangle = -0.81$  for the SMC, and [Mucciarelli \(2014\)](#) reported  $\langle [\alpha/Fe] \rangle \approx +0.10$ .

The full list of adopted population parameters, for all stellar populations discussed in this work, can be found in Table 3.

### 2.2. Theoretical Calibration of the Red Clump

For the theoretical predictions of the color of the red clump, we use the isochrones from the BaSTI database<sup>1</sup>, for both the scaled-solar and  $\alpha$ -enhanced ( $[\alpha/Fe] = +0.40$ )

<sup>1</sup> <http://basti.oa-abruzzo.inaf.it/index.html>

cases (Pietrinferni et al. 2004, 2006; Cordier et al. 2007). We use the models with the suggested opacities (Ferguson et al. 2005) and with red giant mass loss parameter of  $\eta = 0.20$  (Reimers 1975). This value has been validated by Miglio et al. (2012) in their study of NGC 6791 and 6819, two open clusters for which there are asteroseismic data. We use isochrones with the metallicities  $[M/H] = \{-0.66, -0.35, -0.25, +0.06, +0.26, +0.40\}$  and ages  $\tau/\text{Gyr} = \{2.5, 5.0, 10.0, 12.0\}$ , we also include isochrones with  $([Fe/H], [\alpha/Fe]) = (-0.96, 0.00)$ .

The predicted mean color and mean magnitude of the red clump are derived by computing the luminosity function-weighted mean of all equivalent evolutionary points in the isochrone in and near the red clump. We The full range in  $I$  magnitudes is typically 0.15 mag, and adjusting it by 0.01 or 0.02 mag has a negligible impact ( $< 0.01$  mag) on the derived predicted color and magnitude of the red clump. The full list of predicted magnitudes and colors can be found in Table 1, and are plotted in Figure 1.

We find that the dependence of magnitude and color on population parameters cannot be adequately fit for with a simple function over the full parameter space. For example, the dependence of  $(V - I)_{RC,0}$  on age is itself a function of metallicity, see Figure 1. In order to estimate the prediction for the LMC directly from the isochrones, without first deriving empirically-calibrated offsets, we compute a linear fit over a limited parameter range, with  $[Fe/H] \leq -0.25$ ,  $2.5 \leq \tau/\text{Gyr} \leq 10$ :

$$(V - I)_{RC,0,LMC} = 0.92 + 0.20([Fe/H]_{LMC} + 0.64) + 0.12([\alpha/Fe]_{LMC} - 0.03) + 0.01 \log(\tau_{LMC}/6 \text{ Gyr}) \quad (1)$$

$$M_{I,RC,LMC} = -0.42 + 0.19([Fe/H]_{LMC} + 0.64) + 0.06([\alpha/Fe]_{LMC} - 0.03) + 0.36 \log(\tau_{LMC}/6 \text{ Gyr}), \quad (2)$$

where the x-intercepts are chosen to correspond to the population parameters of the LMC. Similarly for the SMC, we compute a linear fit over a limited parameter range, with  $[Fe/H] \leq -0.60$ ,  $\tau/\text{Gyr} \leq 10$ :

$$(V - I)_{RC,0,SMC} = 0.87 + 0.18([Fe/H]_{SMC} + 0.88) + 0.09([\alpha/Fe]_{SMC} + 0.02) + 0.00 \log(\tau_{SMC}/5 \text{ Gyr}) \quad (3)$$

$$M_{I,RC,SMC} = -0.50 + 0.15([Fe/H]_{SMC} + 0.88) + 0.07([\alpha/Fe]_{SMC} + 0.02) + 0.39 \log(\tau_{SMC}/5 \text{ Gyr}), \quad (4)$$

The scatter between the model-predicted values and the fit-predicted values is  $\sim 0.01$  mag.

The predicted theoretical dependence of  $(V - I)_{RC,0}$  on age and metallicity is plotted in Figure 1, where we also

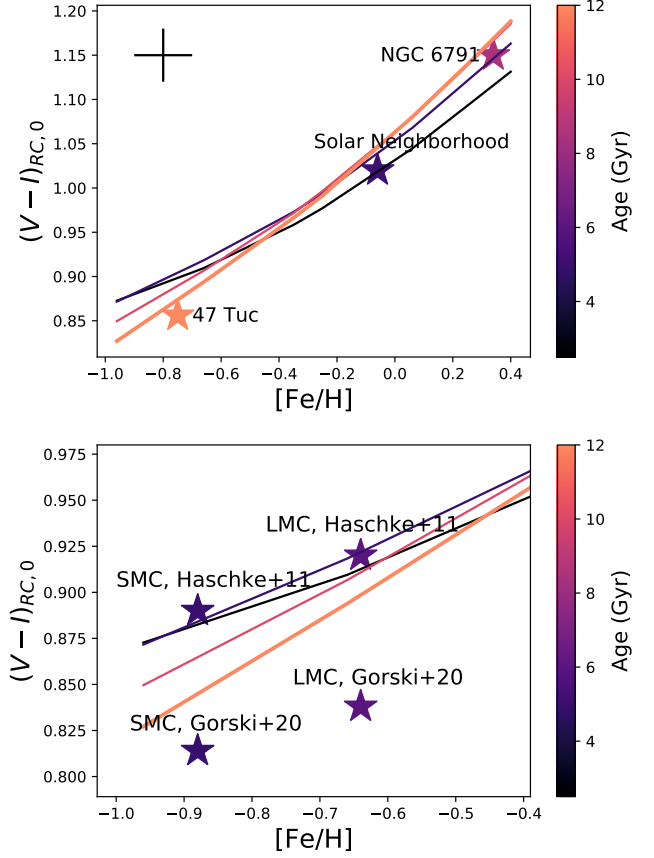


**Figure 1.** The BaSTI-predicted values of  $(V - I)_{RC,0}$  as a function of  $[Fe/H]$  for  $[\alpha/Fe] = 0$  and  $\tau/\text{Gyr} = (2.5, 5.0, 10.0, 12.0)$ , shown as the curves that are color-coded by age. We show the  $(V - I)_{RC,0}$  values for three calibrating stellar populations as asterisks color-coded for ages, with a characteristic error bar shown in the top-left of the plot. The adopted values of  $[Fe/H]$ , age, etc are justified in Section 2.3. The  $(V - I)_{RC,0}$  of 47 Tuc is shifted by 0.025 mag due to its elevated  $\alpha$ -element and initial helium abundance. The measured values of  $(V - I)_{RC,0}$  are on average  $\sim 0.02$  mag lower (bluer) than the BaSTI-predicted values. A zoom-in of the lower-metallicity relationship is shown in the bottom panel, where we also show, as asterisks color-coded for age, the  $(V - I)_{RC,0} = 0.89, 0.92$  values assumed by Haschke et al. (2011) and  $(V - I)_{RC,0} = 0.814 \pm 0.034, 0.838 \pm 0.034$  Górski et al. (2020), with  $[Fe/H]$  and age assumptions justified in Section 2.1.

show the empirical measurements for our three calibrating populations, and the previously assumed parameters for the LMC and SMC.

We did verify how increasing the color range to the red to include the first ascent red giant branch would shift the derived colors. That is in principal more appropriate for composite populations such as the LMC, the SMC, and the Solar Neighbourhood, for which the red clump is inevitably mixed with the first ascent red giant branch. We found that the effect is small – the predicted  $(V - I)_{RC,0}$  is increased by

0.005 mag. That is because of the relative number counts of the two phases. Nataf et al. (2014) computed, using the same isochrones as used here, that the equivalent width of the red clump above the underlying red giant luminosity function is approximately 2.0 magnitudes.

We also list the predictions of the updated BaSTI database<sup>2</sup> (Hidalgo et al. 2018) for four metallicities. We downloaded isochrones with overshooting, diffusion, and mass-loss parameter  $\eta = 0.30$ . This new version of the BaSTI model library represents a significant improvement with respect the previous release. We refer to Hidalgo et al. (2018) for a detailed discussion on the various updates in both the input physics and numerical assumptions adopted for computing the new BaSTI stellar models. However, for the sake of completeness here we mention that version 2 of BaSTI models is based on: an updated solar heavy-elements distribution (Caf-fau et al. 2011), updated nuclear reaction rates for both H- and He-burning phase (see Pietrinferni et al. 2010 and references therein), revised outer boundary conditions, and updated conductive opacity evaluations (Cassisi et al. 2007) as well as an average mass loss efficiency during the RGB stage constrained on the basis of asteroseismic benchmarks (Miglio et al. 2012). In particular, we note that the use of updated conductive opacity and a different mass loss efficiency directly impacts on the RC average color and magnitude, as will be shown in the following sections. Ideally, these isochrones would be used for all of the calculations, but their grid for the  $\alpha$ -enhanced heavy element distribution is not yet available.

The different predictions are listed in Table 2. The predictions for the red clump from these updated models are consistently 0.13 mag fainter in  $M_{I,RC}$ , and 0.03 mag bluer in  $(V - I)_{RC,0}$ , relative to those of BaSTI version 1.0.

### 2.3. Empirical Measurements of the color of the Red Clump

In the prior section, we predicted the slope and zero-point of the color-metallicity relation of the red clump. In this subsection, we use the measured color-magnitude diagrams of three stellar populations in the Milky Way to verify their accuracy. These are the globular cluster 47 Tuc (NGC 104), the solar neighbourhood stellar population, and the open cluster NGC 6791. These populations are selected as they host numerous red clump stars, and they are well-characterized in distance, reddening, and population parameters such as metallicity. They also provide a broad span in  $[\text{Fe}/\text{H}]$  which brackets the Magellanic Clouds. The color-magnitude diagrams of 47 Tuc and NGC 6791 are shown in Figure 2.

The population parameters that we adopt are derived from a range of methods and data sets. There is unfortunately no uniformly-derived set of population parameters available across these different populations. Thus we adopt the most tightly calibrated parameters available for the distances, reddening, metallicity, and age determinations (Table 2).

[Fe/H]	[ $\alpha$ /Fe]	$\tau$ /Gyr	$M_{I,RC}$	$(V - I)_{RC,0}$
-1.01	0.40	2.50	-0.60	0.89
-1.01	0.40	5.00	-0.51	0.90
-1.01	0.40	10.00	-0.37	0.88
-1.01	0.40	12.00	-0.32	0.86
-0.96	0.00	2.50	-0.63	0.87
-0.96	0.00	5.00	-0.53	0.87
-0.96	0.00	10.00	-0.36	0.85
-0.96	0.00	12.00	-0.29	0.83
-0.70	0.40	2.50	-0.54	0.94
-0.70	0.40	5.00	-0.45	0.95
-0.70	0.40	10.00	-0.33	0.94
-0.70	0.40	12.00	-0.30	0.94
-0.66	0.00	2.50	-0.59	0.91
-0.66	0.00	5.00	-0.48	0.92
-0.66	0.00	10.00	-0.34	0.91
-0.66	0.00	12.00	-0.29	0.89
-0.60	0.40	2.50	-0.52	0.96
-0.60	0.40	5.00	-0.43	0.97
-0.60	0.40	10.00	-0.32	0.97
-0.60	0.40	12.00	-0.28	0.96
-0.35	0.00	2.50	-0.50	0.96
-0.35	0.00	5.00	-0.40	0.97
-0.35	0.00	10.00	-0.29	0.97
-0.35	0.00	12.00	-0.25	0.97
-0.29	0.40	2.50	-0.44	1.03
-0.29	0.40	5.00	-0.37	1.06
-0.29	0.40	10.00	-0.27	1.07
-0.29	0.40	12.00	-0.24	1.06
-0.25	0.00	2.50	-0.47	0.98
-0.25	0.00	5.00	-0.38	0.99
-0.25	0.00	10.00	-0.26	1.00
-0.25	0.00	12.00	-0.23	0.99
-0.09	0.40	2.50	-0.42	1.09
-0.09	0.40	5.00	-0.34	1.12
-0.09	0.40	10.00	-0.25	1.13
-0.09	0.40	12.00	-0.23	1.13
0.05	0.40	2.50	-0.41	1.14
0.05	0.40	5.00	-0.34	1.18
0.05	0.40	10.00	-0.25	1.19
0.05	0.40	12.00	-0.22	1.20
0.06	0.00	2.50	-0.37	1.04
0.06	0.00	5.00	-0.28	1.07
0.06	0.00	10.00	-0.19	1.08
0.06	0.00	12.00	-0.16	1.08
0.25	0.00	2.50	-0.32	1.09
0.25	0.00	5.00	-0.24	1.12
0.25	0.00	10.00	-0.15	1.14
0.25	0.00	12.00	-0.12	1.14
0.40	0.00	2.50	-0.30	1.13
0.40	0.00	5.00	-0.22	1.16
0.40	0.00	10.00	-0.14	1.19
0.40	0.00	12.00	-0.11	1.19

**Table 1.** The mean magnitude and color of the red clump as predicted by the BaSTI isochrones for a range of population abundances and ages.

[Fe/H]	$\tau/\text{Gyr}$	$M_{I,RC}$	$(V-I)_{RC,0}$	$M_{I,RC}$	$(V-I)_{RC,0}$
-0.96	5.00	-0.53	0.87	-0.44	0.84
-0.96	10.00	-0.36	0.85	-0.18	0.79
-0.35	5.00	-0.40	0.97	-0.31	0.95
-0.35	10.00	-0.29	0.97	-0.15	0.94
0.06	5.00	-0.28	1.07	-0.17	1.05
0.06	10.00	-0.19	1.08	-0.04	1.06
0.25	5.00	-0.24	1.12	-0.11	1.11
0.25	10.00	-0.15	1.14	0.01	1.12

**Table 2.** The third and fourth columns list the predictions of the old BaSTI database (Pietrinferni et al. 2004, 2006; Cordier et al. 2007), and the 5th and 6th columns list the predictions of the updated BaSTI database (Hidalgo et al. 2018). The updated physics lead to predictions for the red clump that are consistently 0.13 mag fainter in  $M_{I,RC}$ , and 0.03 mag bluer in  $(V-I)_{RC,0}$ .

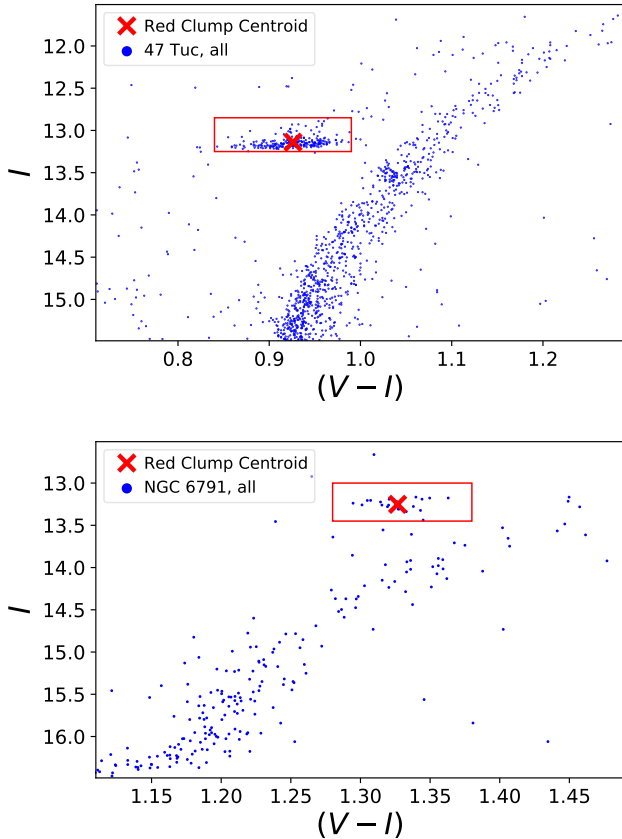


**Figure 2.** The color-magnitude diagrams of 47 Tuc (TOP) and NGC 6791 (BOTTOM). The stars selected as being part of the red clump are plotted in the red rectangles.

### 2.3.1. 47 Tuc

For 47 Tuc, we use the color-magnitude diagram of Bergbusch & Stetson (2009), and we restrict the sample to those stars with angular separation from the cluster cen-

ter of  $(\alpha, \delta) = (6.023625, -72.081276)^2$ , in arcseconds, of  $400 \leq \delta\psi \leq 900$ , in order to reduce the effect of blending. We select the 241 red clump stars satisfying  $0.84 \leq (V-I) \leq 0.99$  and  $12.85 \leq I \leq 13.25$ , for mean apparent photometry of  $(V-I)_{RC} = 0.927 \pm 0.002$  and  $I_{RC} = 13.139 \pm 0.004$ . The value of this measured centroid is negligibly sensitive to the dimensions of the box, as shifting the box 0.02 mag in color or 0.03 mag in magnitude has a 0.001 mag effect on each of  $(V-I)_{RC}$  and  $I_{RC}$ . We have verified that we obtain a nearly identical result,  $(V-I)_{RC} = 0.913 \pm 0.001$  and  $I_{RC} = 13.086 \pm 0.003$ , if we had instead used the color-magnitude diagram of Sarajedini et al. (2007), which is obtained from highly accurate and highly-precise Hubble Space Telescope observations in  $F606W$  and  $F814$  transformed into  $V$  and  $I$  using theoretical transformations. The slightly bluer and brighter horizontal branch is likely due to the gradient in helium enrichment in the cluster (Nataf et al. 2011; Milone et al. 2012).

For the apparent distance, reddening to, and age of 47 Tuc, we adopt the values of  $(m-M)_V = 13.370 \pm 0.015$ ,  $E(V-I) = 0.045 \pm 0.01$ , and  $\tau = 12.0$  Gyr from Thompson et al. (2020). These measurements are predominantly derived from spectroscopic and photometric measurements of four members of two eclipsing binary systems. The value and error of the distance modulus are computed from the values of the four eclipsing binary members. That is somewhat unphysical, as the errors on those four individual distances are almost certainly correlated (or anti-correlated), but unfortunately both the sign and amplitude of that correlation are unknown.

We estimate the population abundances from APOGEE spectra of 60 cluster stars, where we use the cluster selection criteria as Nataf et al. (2019), we require  $\log g \leq 3.0$ , and we restrict the analysis to stars satisfying  $[\text{N}/\text{Fe}] \leq +0.35$ , a parameter space for which the consistency of the ASPCAP pipeline with other literature estimates has been demonstrated (Jönsson et al. 2018). We obtain the median abundances of  $[\text{Fe}/\text{H}] = -0.75$  and  $[\alpha/\text{Fe}] = +0.26$ .

Our assumed population parameters for 47 Tuc are consistent with other literature values. From Thygesen et al. (2014), Johnson et al. (2015), and Marino et al. (2016) we respectively find  $([\text{Fe}/\text{H}], [\text{Mg}/\text{Fe}], [\text{Ca}/\text{Fe}]) = (-0.78, +0.44, +0.24)$ ,  $([\text{Fe}/\text{H}], [\text{Mg}/\text{Fe}]) = (-0.73, +0.33)$ , and  $[\text{Fe}/\text{H}] = -0.68$ . The distance ( $\mu = 13.29$ ) is a little higher than the value of  $\mu = 13.23 \pm 0.02$  derived by Baumgardt et al. (2019) from Gaia DR2 data. Salaris et al. (2016) estimated  $\mu \approx 13.33$  by matching the observed red clump stellar distribution with models constructed from the same stellar evolution code used

<sup>2</sup> Taken from <https://people.smp.uq.edu.au/HolgerBaumgardt/globular/orbits.html>, for details see Baumgardt et al. (2019).

Population	[Fe/H]	[ $\alpha$ /Fe]	$\tau$ /Gyr	$(m - M)_V$	$E(V - I)$	$(V - I)_{RC,0}$	$(V - I)_{RC,BaSTI}$	$M_{I,RC}$	$M_{I,RC,BaSTI}$
47 Tuc (NGC 104)	-0.75	+0.26	12	13.37	0.045	0.88	0.90	-0.18	-0.34
Large Magellanic Cloud	-0.64	+0.03	6	-	-	-	0.91	-	-0.42
Small Magellanic Cloud	-0.88	-0.02	5	-	-	-	0.88	-	-0.49
Solar Neighborhood	-0.06	+0.04	5.1	-	-	1.02	1.05	-0.23	-0.32
NGC 6791	+0.34	+0.04	8.3	13.51	0.174	1.15	1.17	-0.08	-0.17

**Table 3.** In the four right-most columns, we show both the best-fit measured intrinsic parameters of the red clump, and the BaSTI-predicted parameters of the red clump. The measured parameters assume the distance and reddening values shown in the 5th and 6th columns, and the predicted parameters assume the chemistry and age values shown in the 2nd, 3rd, and 4th columns. For our three comparisons, the BaSTI-predicted values are on average  $\sim 0.02$  mag redder in  $(V - I)$ , and  $\sim 0.11$  mag brighter in  $M_I$ .

in this work, but with a different prescription concerning the mass loss efficiency during the red giant branch stage. Finally, Hansen et al. (2013) estimated an age of  $\tau/\text{Gyr} = 9.9 \pm 0.7$  from its white dwarf cooling sequence. Grundahl et al. (2002) used stromgren photometry of the cluster to estimate  $(m - M)_V = 13.33$ ,  $E(B - V) = 0.04$ , and an age of  $\tau/\text{Gyr} = 12$ .

The stellar population of 47 Tuc is also characterized by a small spread in initial helium abundance  $Y$  (di Criscienzo et al. 2010; Nataf et al. 2011; Milone et al. 2017, 2018). Indeed, Gratton et al. (2013) studied the spectra of 110 red clump stars in 47 Tuc and found the  $[\text{Na}/\text{O}]$  abundances – and thus by proxy, the initial helium abundances – were tightly anti-correlated with the  $(B - V)_0$  colors. Salaris et al. (2016) showed that the standard deviation in color and magnitude of the red clump of 47 Tuc is matched well by varying the initial helium abundance of the cluster’s stars to be uniformly distributed in the interval  $Y \in [0.256, 0.286]$ . Using the BaSTI database, we find that this will shift the predicted red clump to being bluer and brighter, by  $(\Delta(V - I)_{RC,0}, \Delta M_{I,RC}) = (-0.009, -0.042)$ . We find the predicted properties of the red clump in 47 Tuc are thus  $((V - I)_{RC,0}, M_{I,RC}) = (0.899, -0.336)$ . In contrast, the observed values are  $((V - I)_{RC,0}, M_{I,RC}) = (0.882, -0.186)$ .

### 2.3.2. Solar Neighborhood

For the solar neighbourhood, Chan & Bovy (2019) have measured mean values of  $M_{RC,J} = -1.019$  and  $M_{RC,K_s} = -1.622$ . However, the selection function that they used assumes the APOGEE red clump catalog (Bovy et al. 2014), which incorporates spectroscopic priors. That may differ from the photometric definition of the red clump used for populations such as the LMC and SMC, which is an excess in the luminosity function of post-main-sequence stars at or very close to the location of the horizontal branch.

We produced a photometric selection of Red Clump stars in the solar neighborhood by the following steps. We used the Gaia (Gaia Collaboration et al. 2016) Data Release 2 (Lindegren et al. 2018) solar neighbour-

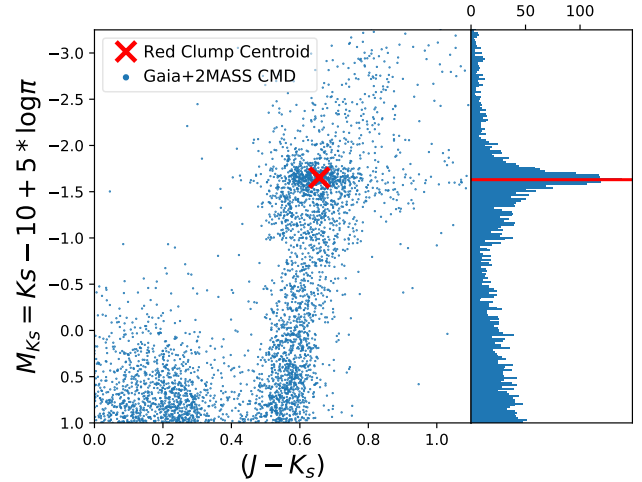


**Figure 3.** LEFT: The  $(J - K_s, M_{K_s})$  color-magnitude diagram of solar neighbourhood stars within  $\sim 300$  pc, with  $\delta \geq -30^\circ$ . We plot every 5th data point for purposes of clarity. RIGHT: The  $M_{K_s}$  luminosity function of the red giant branch stars, the red clump is measured to have a peak magnitude of  $M_{K_s} = -1.63$ .

hood measurements from the Gaia archive<sup>3</sup>, where we used their cross-match to the 2MASS catalog (Skrutskie et al. 2006). We required  $visibility\_periods\_used > 5$ ,  $astrometric\_excess\_noise < 1$ , and apply a zero-point offset to the parallaxes of  $\delta\pi = -0.054$  mas (Schönrich et al. 2019). We select nearby stars with precise parallax measurements, such that  $\pi \geq 3$  and  $\pi/\sigma_\pi \geq 100$ .

We selected a low-reddening sample by requiring that the estimated reddening to the stars satisfies  $E(g - r) \leq 0.04$  (Green et al. 2019), for a mean reddening of  $\langle E(g - r) \rangle = 0.005$ , or equivalently,  $\langle E(J - K_s) \rangle = 0.003$  (Fitzpatrick 1999). We use the fitting routine of Nataf et al. (2016) to measure the properties of the red clump sample as an excess in the luminosity function over that of red giant stars, a method first developed by Stanek et al. (1997) and Paczyński & Stanek (1998). This selects approximately 1500 red clump stars. We

<sup>3</sup> <https://gea.esac.esa.int/archive/>

note that the stars used in our analysis are not themselves inputs into the 3D reddening maps of Green et al. (2019), as those maps are constructed from stars fainter than the saturation limits of Pan-STARRS 1 (Flewelling et al. 2016).

To link measurements in  $(J, K_s)$  to expected colors in  $(V, I)$ , we use the color-color relations from Table 1 of Nataf et al. (2016), which are derived from the library of synthetic stellar colors of Casagrande & Vandenberg (2014).

Our best-fit values for the solar neighborhood red clump are thus  $M_{RC,K_s} = -1.63$ ,  $\sigma_{M_{K_s}} = 0.14$ ,  $(J - K_s) = 0.64$ ,  $M_{RC,I} = -0.23$ , and  $(V - I) = 1.02$ , where the statistical errors are each less than 0.01 mag. The  $((V - I)_{RC,0}, M_{I,RC})$  compare well to the prior measurement of  $M_{RC,I} - 0.28$ , and  $(V - I) = 1.01$  from Paczyński & Stanek (1998), which was derived from Hipparcos data (Perryman et al. 1997). The zero-point shift in the parallaxes of  $\delta_\pi = -0.054$  mas (Schönrich et al. 2019) shifts  $M_{RC,K_s}$  by 0.03 mag. If we instead adopt the distances of Bailer-Jones et al. (2018), which assume priors for Galactic geometry discussed in that work, a zero point offset to the Gaia parallaxes of  $\delta_\pi = -0.029$  (Lindegren et al. 2018), we obtain the same color, but a slightly brighter red clump, with  $M_{RC,K_s} = -1.64$ . We thus suggest a 0.01 mag error on  $M_{K_s}$ , due to this ambiguity as to which small correction we should apply to the DR2 parallaxes.

We also derive the following colors for the solar neighborhood red clump, by direct fitting to the Gaia and 2MASS data:  $(G_{BP} - K_s) = 2.75$ ,  $(G - K_s) = 2.18$ ,  $(G_{RP} - K_s) = 1.52$ , and  $(H - K_s) = 0.15$ .

The color-magnitude diagram of solar neighbourhood stars selected to have low reddening, and the combined red giant and red clump luminosity function, is shown in Figure 3.

The solar neighbourhood population parameters that we assume,  $(\langle[Fe/H]\rangle, \langle[\alpha/Fe]\rangle, \langle\tau/\text{Gyr}\rangle) = (-0.06, +0.04, 5.1)$  are from Feuillet et al. (2019), who computed posterior age distributions for  $\sim 20,000$  APOGEE targets with Galactic positions satisfying  $7 \leq R_{GC}/\text{kpc} \leq 9$ , and  $|z| \leq 0.50\text{kpc}$ . These are remarkably similar to the values of  $(\langle[Fe/H]\rangle, \langle[\alpha/Fe]\rangle, \langle\tau/\text{Gyr}\rangle) = (-0.06, +0.03, 5.1)$  derived by Buder et al. (2019) from GALAH survey data (De Silva et al. 2015).

The predicted solar neighbourhood red clump color and magnitude, assuming the parameters from Feuillet et al. (2019), fitting over the full span of Table 1, are  $((V - I)_{RC,0}, M_{I,RC}) = (1.05, -0.32)$ . In contrast, the observed values are  $((V - I)_{RC,0}, M_{I,RC}) = (1.02, -0.25)$ .

### 2.3.3. NGC 6791

For NGC 6791, we use the color-magnitude diagram of Stetson et al. (2003), which was updated for the work of Brogaard et al. (2012) and now includes corrections for differential reddening. We limit the selection to stars with Gaia-derived proper motions that are within 1.25 mas of the clus-

ter central value of  $\mu_\alpha \cos\delta$ ,  $\mu_\delta = (-0.42, -2.28)$  reported by Donor et al. (2018). We select 24 red clump stars that have  $1.24 \leq (V - I) \leq 1.38$  and  $13.45 \leq I \leq 13.00$ , for mean apparent photometry of  $((V - I)_{RC}, I_{RC})_{\text{NGC 6791}} = (1.327 \pm 0.003, 13.252 \pm 0.013)$ . The value of this measured centroid is negligibly sensitive to the dimensions of the box, as shifting the box to remove the bluest point, which does appear as the most uncertain point, reduces  $(V - I)_{RC}$  by 0.002 mag and increases  $I_{RC}$  by 0.003 mag effect. The color-magnitude diagram of NGC 6791 is shown in the bottom panel of Figure 2.

The analysis of Brogaard et al. (2012), which incorporates information from the masses and radii of eclipsing binaries as well as the morphology of the three-bandpass color-magnitude diagram, yields the cluster parameters of  $(m - M)_V = 13.51 \pm 0.06$ ,  $E(V - I) = 0.17 \pm 0.02$ , and  $\tau = 8.3$  Gyr. The value and error of the distance modulus is computed from the values of the four eclipsing binaries listed in Table 1 of Brogaard et al. (2012). That is somewhat unphysical, as the errors on those four individual distances are almost certainly correlated (or anti-correlated), but unfortunately both of the sign and amplitude of that correlation are not available. From APOGEE spectra, the median abundances of 55 cluster stars with surface gravity  $\log g \leq 3.0$  are  $[Fe/H] = +0.34$ ,  $[\alpha/Fe] = +0.04$ .

These adopted population parameters are consistent with other literature values. Boesgaard et al. (2015) measured  $(\langle[Fe/H]\rangle, \langle 1/5[O+Mg+Si+Ti+Ca/Fe]\rangle) = (+0.30, -0.02)$ , and Villanova et al. (2018) measured  $(\langle[Fe/H]\rangle, \langle 1/4[Mg+Si+Ti+Ca/Fe]\rangle) = (+0.31, +0.06)$ . García-Berro et al. (2010) estimated an age of 8 Gyr from analysis of the cluster's white dwarf cooling sequence, and McKeever et al. (2019) estimated an age of  $\tau/\text{Gyr} = 8.2$  from an asteroseismic analysis of the cluster's giants. One discrepant result is that of An et al. (2015), who applied the method of main-sequence fitting to  $BVI_cJHK_s$  photometric data of the cluster, and derived best-fit values of  $[M/H] = +0.42$ ,  $(m - M)_V = 13.38$ ,  $E(V - I) = 0.137$ , and  $\tau/\text{Gyr} = 9.5$ . Anthony-Twarog et al. (2007) used stromgren photometry of the cluster to  $[Fe/H] = +0.45$   $(m - M)_V = 13.60$ ,  $E(B - V) = 0.155$ , and an age of  $\tau/\text{Gyr} = 7$ .

Using predicted parameters from Table 3 satisfying  $5 \leq \tau/\text{Gyr} \leq 10$  Gyr,  $[Fe/H] \geq 0$ , we find that the predicted NGC 6791 red clump has  $((V - I)_{RC,0}, M_{I,RC}) = (1.17, -0.17)$ . In contrast, the dereddened observed values are  $((V - I)_{RC,0}, M_{I,RC}) = (1.15, -0.09)$ .

### 2.4. A Combined Theoretical and Empirical Prediction for the Red Clumps of the Magellanic Clouds

The offsets between theory and data for the three stellar populations used in this work are highly consistent which supports the use of empirical re-calibration of the models. For

47 Tuc, the solar neighborhood, and NGC 6791, we measure red clumps that are respectively 0.02, 0.03, and 0.02 mag bluer in  $(V - I)$ , and 0.16, 0.09, and 0.09 mag fainter in  $M_I$ , relative to the model predictions, as listed in Table 1 and Equations (1), (2), (3), and (4). The offset between the data and the old BaSTI models is nearly equal to the offset between the old BaSTI models and the updated BaSTI models, where the latter are typically  $\sim 0.03$  mag bluer and  $\sim 0.13$  mag fainter.

Assuming these mean offsets of 0.02 mag and 0.11 mag, we derive predicted colors and magnitudes for the Magellanic Clouds of  $((V - I)_{RC,0,LMC}, M_{RC,I,LMC}) = (0.90, -0.31)$  and  $((V - I)_{RC,0,SMC}, M_{RC,I,SMC}) = (0.85, -0.39)$ .

### 3. VERIFYING THE CONSISTENCY OF OUR ABSOLUTE MAGNITUDE AND INTRINSIC COLOR CALIBRATIONS

The independent calibrations of the absolute magnitude and intrinsic color of the red clump enable us to verify that our estimates are consistent with one another. By definition,

$$\mu = I_{RC} - M_{I,RC} - A_I, \quad (5)$$

where  $I_{RC}$  is the apparent magnitude of the red clump, and  $A_I$  is the extinction in  $I$ -band along a sightline. If we assume a standard extinction curve, then,  $A_I = 1.31E(V - I)$  (Fitzpatrick 1999), and therefore:

$$\mu = I_{RC} - M_{I,RC} - 1.31((V - I)_{RC} - (V - I)_{RC,0}). \quad (6)$$

We downloaded the OGLE-III photometry for the LMC fields 100.1 and 101.1 (Udalski et al. 2008a). These sightlines were selected to be towards the center of the LMC, enabling us to compare our result to the measured distance for that galaxy, without needing to correct for a geometric tilt.

We derive  $\mu_{LMC} \approx 18.44$ , which is close to the value of  $\mu_{LMC} = 18.48$  measured from the analysis of twenty eclipsing binary systems (Pietrzyński et al. 2019).

This method, when applied to the SMC photometry (Udalski et al. 2008b), did not yield as unambiguous a test as it did for the LMC. The red clump of the SMC appears to have a substantially more skew-symmetric magnitude distribution than that of the LMC. If we use the mean of the magnitudes of the red clump, we derive  $\mu_{SMC} \approx 18.76$ , whereas if we use the mode we derive  $\mu_{SMC} \approx 18.94$ . It is only the latter that is consistent with the standard value of  $\mu_{SMC} = 18.95 \pm 0.07$ , that is measured from the analysis of four eclipsing binary systems Graczyk et al. (2014). An assessment of consistency in this case will thus require a much more detailed analysis of the color-magnitude diagram of the SMC.

We note that there is some history behind the work done in this Section. Some of the first distances estimates to the Magellanic Clouds derived from photometry of red clump stars yielded a ‘‘short distance scale’’, with  $\mu_{LMC} = 18.08$

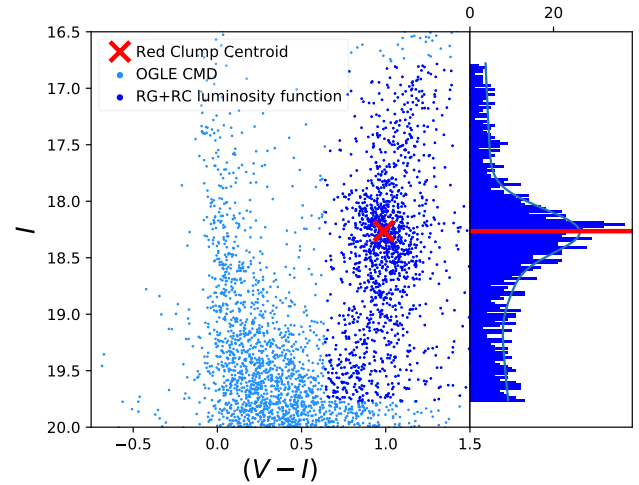


**Figure 4.** OGLE-III Color-magnitude diagram and luminosity function of part of the field lmc100.1. The combination of intrinsic red clump properties estimated in this work, with its apparent properties estimated from the color-magnitude diagram, yield a distance modulus of  $\mu_{LMC} = 18.44$ , consistent with the standard value of  $\mu_{LMC} = 18.48$  (Pietrzyński et al. 2019).

and  $\mu_{SMC} = 18.56$  (Udalski et al. 1998), and separately,  $\mu_{LMC} = 18.36$  and  $\mu_{SMC} = 18.82$  (Cole 1998). The reason for this discrepancy is partially the requirement to account for population effects (metallicity, age, etc) on the optical properties of the red clump (Girardi & Salaris 2001; Percival & Salaris 2003), and partially that it was not clear how to account for these population effects. This was confirmed with the observations of the red giant branches of 15 local group dwarfs by Pietrzyński et al. (2010).

### 4. THE REDDENING TOWARD THE MAGELLANIC CLOUDS

The Magellanic Clouds are among the best-studied sightlines in astronomy, and thus we have multiple options available to use independent tracers to test the available reddening maps derived from different choices for the color of the red clump. In this investigation, we use newly available observations of the colors of LMC Cepheids observed with *HST*, classical Cepheids observed from the ground, and RR Lyrae stars of the ab-type observed from the ground.

#### 4.1. Calibration with Cepheids Observed with *HST*

*HST* provides unmatched resolution and stability to overcome errors in Cepheid photometry which reside in some ground-based data due to crowding and zeropoint variations in the LMC (Yuan et al. 2019). We use the newly available sample of 79 LMC Cepheids observed by Riess et al. (2019) as an independent standard crayon. These Cepheids have been observed in the WFC3-UVIS optical bands  $F555W$  and  $F814W$ , in two *HST* programs: GO-14648 and GO-15146 (PI: Riess) across the LMC. The color  $F555W - F814W$  is the

same  $V - I$  color studied here to evaluate LMC reddening and the dispersion of the *HST* colors is about 25% lower around a period-color relation than ground-measured Cepheids from OGLE, providing a sharp test of the red clump maps. We exclude two Cepheids, OGLE1940 and OGLE1945 with colors of 1.3 and 1.6 mag, 5 and 8  $\sigma$  from the mean and indicative of high circumstellar reddening which is distinct from the interstellar reddening measured by the maps.

We adopt two independent benchmarks for the unreddened Cepheid  $F555W - F814W$  period-color relations. The first is empirical, from Macri et al. (2006). They used *HST* data to study Cepheids in the nearby maser-host galaxy NGC 4258. Their sample includes 57 Cepheids with periods from 3 to 44 days toward an outer region,  $\sim 20$  Kpc from the center of that galaxy where the host reddening should be minimal and the mean metallicity is  $[O/H]=8.65$ , similar to the LMC (Riess et al. 2016). The foreground reddening is also very low,  $E(V - I) = 0.022$ , leaving little residual uncertainty after its removal. We fit a linear  $P - C$  relation to this data which yields  $F555W - F814W = 0.60 + 0.31(\text{Log}P)$ .

The second unreddened benchmark is from the work of Fiorentino et al. (2013), who computed theoretical period-color relations from stellar pulsational models in the WFC3  $F555W - F814W$  system. Their predictions for various compositions can be found in their Table 1. We use the entry from that Table that they recommend for the LMC, which is computed from stellar models with initial metals abundance  $Z = 0.008$  and initial helium abundance  $Y = 0.25$  and yields  $F555W - F814W = 0.59 + 0.31(\text{Log}P)$ , the same slope as the empirical relation and bluer by 0.01 mag.

In Figure 5, we plot the LMC Cepheid color  $F555W - F814W$  as observed vs log Period/days. We further show the colors after the Cepheid sight lines individually corrected by the reddening map of Haschke et al. (2011), by a reddening map derived from RR Lyrae (described in Section 4.3), and by the reddening map of Górski et al. (2020) based on a bluer red clump color.

In each of the four panels, the reddening-free empirical period-color relation (Macri et al. 2006), is shown as the blue line, and the theoretical period-color relation (Fiorentino et al. 2013) is shown as the red line which are quite similar.

Without dereddening (top-left panel), the observed period-color relation (the black line) lies at redder colors than the theoretical prediction of (Fiorentino et al. 2013), by a mean of 0.053 mag in  $F555W - F814W$ , which approximately corresponds to 0.06 mag in  $E(V - I)$  (Fitzpatrick 1999). It is not surprising that the best linear fit to the observed data is parallel but redder than the predicted intrinsic best fit as reddening of Cepheids by the LMC is expected. We are impressed that the mean of  $E(V - I) = 0.06$  (top-right panel) is close to the mean reddening  $E(V - I) = 0.068$  predicted by the maps of Haschke et al. (2011) and from

the RR Lyrae based reddening map (bottom-left panel). In contrast, the mean reddening from the maps of Górski et al. (2020) is  $E(V - I) = 0.15$ . As can be seen in the bottom-right panel, it clearly over-predicts the reddening of the *HST* Cepheids. This is not surprising since the maps of Górski et al. (2020) are based on sight lines of Blue Supergiants which are much younger and likely closer to the dusty clusters where they were born as discussed in Section 5.

The use of the *HST*-measured Cepheids as an independent standard crayon with which to study the reddening toward the LMC, under the assumption that the reddening toward Cepheids is on average the same as that toward red clumps, thus suggests zero point color of the red clump of  $(V - I)_{RC,0} \approx 0.93 \pm 0.01$  mag.

#### 4.2. Calibration with OGLE Cepheids

We repeat the exercise of the preceding section, but instead of using measurements derived from *HST* data, we use measurements from ground-based data (Macri et al. 2015). These measurements should in principle be less robust, however, i) they are more numerous, with colours measured for 785 rather than 79 Cepheids, and ii) the additional systematic errors that they may have, such as blending, should be similar to those that may be present in the reddening maps, which are derived from ground-based data. We find similar results as with the *HST* Cepheids with the main difference that the implied reddening zero point,  $(V - I)_{RC,0}$ , is reduced by 0.04 mag. The scatters are shown in Figure 6.

#### 4.3. Calibration with RR Lyrae (*ab*-type)

RR Lyrae stars are horizontal branch stars whose location in the Hertzsprung-Russel diagram places them in the instability strip. The relationship between their metallicities, pulsational periods, and  $V I J H K_s$  magnitudes and colors are predicted by stellar theory (Catelan et al. 2004). There are many types of RR Lyrae stars, in this work we use RR Lyrae of the *ab*-type (here after denoted "RRab"). Population effects for RR Lyrae should not be large, as they probe a narrow region in the age-helium-metallicity phase space of stellar populations, typically only old ( $\tau \gtrsim 10$  Gyr) and metal-poor ( $[Fe/H] \lesssim -1.0$ ) stars (Lee et al. 1994; Cassisi et al. 2004).

An RRab star's intrinsic color can be estimated from its pulsational properties and metallicity, which can be measured independently of distance and reddening. We use two different relationships. The first is the theory-derived, widely-used (e.g. of Pietrukowicz et al. 2015; Kunder et al. 2016) relationship of Catelan et al. (2004):

$$(V - I)_{RRab,0} = 0.55 + 1.13 \log(P/(0.60 \text{ days})) + 0.070([Fe/H] + 1.00) + 0.11([Fe/H] + 1.00)^2, \quad (7)$$

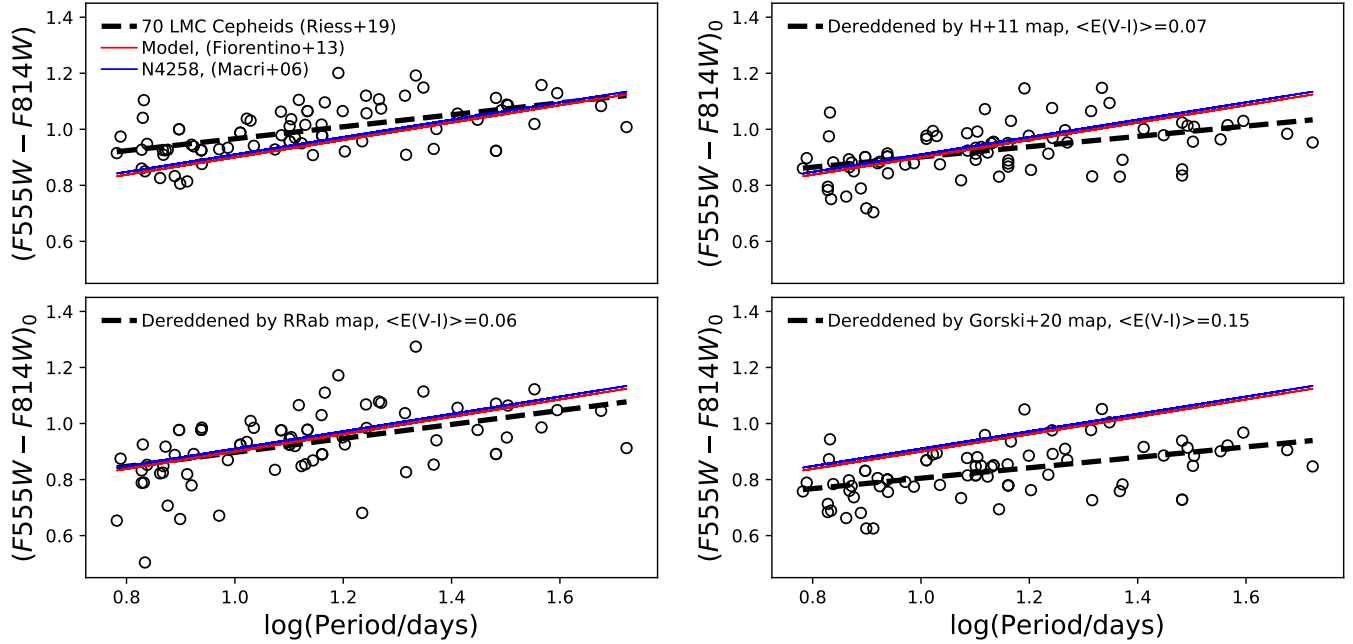


**Figure 5.** The period-color relation of LMC Cepheids (Riess et al. 2019) is shown in the top-left panel assuming no reddening, and in the other three panels assuming three different reddening maps. It is only when using the reddening maps of Haschke et al. (2011) or one from RR Lyrae stars (see Section 4.3) that the observed relation is consistent with independent empirical (Macri et al. 2006) and theoretical (Fiorentino et al. 2013) calibrations. The Cepheid data are thus consistent with LMC reddening maps that assume an intrinsic red clump color of  $(V - I)_{RC,0} \approx 0.93$ .

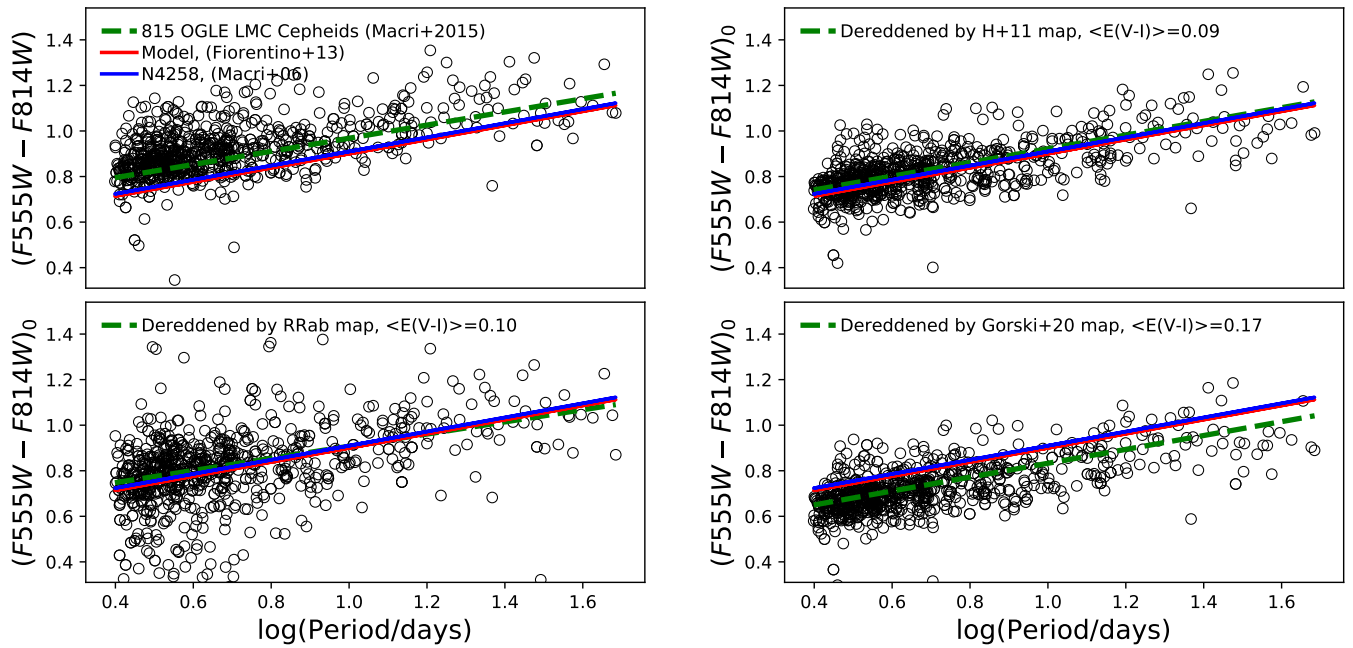


**Figure 6.** Lines and panels as in Figure 5, but with the points being from a compilation of ground-based data of LMC Cepheids by Macri et al. (2015), and with the best-fit to the data drawn as a green rather than a black line.

where the models used by [Catelan et al. \(2004\)](#) assume that  $\log Z = ([\text{Fe}/\text{H}] - 1.765)$ . The second relationship is empirical, which we derive from the compilation of [Monson et al. \(2017\)](#):

$$(V - I)_{\text{RRab},0} = 0.55 + 0.69 \log(P/(0.60 \text{ days})) + 0.032([\text{Fe}/\text{H}] + 1.00), \quad (8)$$

where the metallicities are taken from the work of [Fernley & Barnes \(1997\)](#), and the colors are the intensity-mean magnitudes.

Estimating the metallicities can in turn be done from the Fourier coefficients of the RRab light curves, for which we use the empirical relationship derived by [Smolec \(2005\)](#):

$$[\text{Fe}/\text{H}] = -1.42 - 4.90(P/\text{days} - 0.60) + 0.824(\phi_{31} - 2.51), \quad (9)$$

where  $\phi_{31} = \phi_3 - 3\phi_1$  is a Fourier phase combination for the sine decomposition of the  $I$ -band lightcurve.

We then compare the mean  $E(V - I)$  derived from RRab stars to the values of  $(V - I)_{\text{RC}}$  predicted by [Górski et al. \(2020\)](#). We use RRab stars from the catalog of [Soszyński et al. \(2016\)](#). Both the reddening map of [Górski et al. \(2020\)](#) and the RRab catalog of [Soszyński et al. \(2016\)](#) are on the  $VI$  magnitudes of the OGLE-IV photometric system ([Udalski et al. 2015](#)). We restrict the comparison to RRab stars with  $0.45 \leq P/(\text{days}) \leq 0.80$ , and  $-2.0 \leq [\text{Fe}/\text{H}] \leq 0$ .

Before proceeding we mention a small difference in the calibrations with respect to the data. The evolutionary tracks of [Catelan et al. \(2004\)](#) assume  $[\alpha/\text{Fe}] = 0$ , which is consistent with the measurement for metal-poor stars in the SMC and LMC ([Nidever et al. 2019](#)). In contrast, both of Equations 8 and 9 are empirically calibrated off of Galactic metal-poor stars, for which  $\langle[\alpha/\text{Fe}]\rangle \approx +0.30$ . In principle, the effect should cancel to first order. The  $\alpha$ -enhancement should act to increase the bulk metallicity  $[M/\text{H}]$  for both of Equations 8 and 9, and regardless, the metallicity dependence in Equation 8 is very small. A metallicity difference of  $\Delta[M/\text{H}] = 0.30$  dex – surely an overestimate of the effect of  $\Delta[\alpha/\text{Fe}] \approx 0.30$  dex – amounts to  $\Delta(V - I)_{\text{RRab},0} \approx 0.01$  mag.

Separately, we find that the  $(V - I)_{\text{RRab},0}$  colors predicted by Equation 8 are greater than those predicted by Equation 7, by 0.01 mag for LMC RR stars, and by 0.00 mag for SMC RR Lyrae. The standard deviation in the difference between the predicted colors is  $\sim 0.03$  mag.

Wherever we show comparisons with other methods in this work, we use the results derived using Equation 7, rather than Equation 8, as default. That is an arbitrary choice.

The relationships of Equations 7 and 8 necessitate a zero-point shift in the reddening maps of [Górski et al. \(2020\)](#), to values that are 0.093 and 0.107 mag lower for the LMC, and 0.070 and 0.069 mag for the SMC. That in turn yields RRab-calibrated colors for the red clumps of the Magellanic clouds,

$(V - I)_{\text{RC},0} \approx 0.93$  for the LMC, and  $(V - I)_{\text{RC},0} \approx 0.88$  for the SMC.

#### 4.4. Implications for the Reddening of the Tip of the Red Giant Branch in the LMC

The Tip of the Red Giant Branch (TRGB) is a primary distance indicator that is commonly used to measure the distance to galaxies by tracing the stellar population in their halos where extinction is minimal. Because TRGB is not a type of star but rather the maximum luminosity of many red giants it is difficult to calibrate this luminosity without reliable parallaxes for a large number of Red Giants near the tip ([Mould et al. 2019](#)). Instead, TRGB is most commonly calibrated in the LMC using its measured distance. Unfortunately TRGB stars in the LMC suffer substantial extinction in the  $I$ -band and thus the calibration of TRGB in the halos depends directly on the estimate of the absolute (i.e., true, not differential) LMC extinction or reddening. Here we consider the estimate of the LMC TRGB extinction in light of the red clump calibration from §2.

The reddening maps from [Haschke et al. \(2011\)](#) yield a mean value of  $A_I = 0.10$  (mag) for the sight lines of stars near the TRGB as determined by [Jang & Lee \(2017a,b\)](#) and [Yuan et al. \(2019\)](#) which were derived from a value of  $(V - I)_{\text{RC},0} = 0.92$ , consistent with the values found here. This extinction calibration leads to  $M_{I,\text{TRGB}} = -3.97 \pm 0.03$  based on the DEB distance to the LMC of  $m - M = 18.477$  ([Pietrzyński et al. 2019](#)) and an apparent  $m_{I,\text{TRGB}} = 14.60$ .

For an independent comparison, we measured the extinction of TRGB sight lines from LMC reddening maps derived from RR Lyrae star colors. RR Lyrae should provide very good tracers for TRGB extinction as they are similar in age and are good calibrated crayons. We measured the median reddening of the TRGB sight lines (TRGB samples from [Jang & Lee \(2017a,b\)](#) and [Yuan et al. \(2019\)](#)) using the RR Lyrae LMC reddening maps discussed in §4.3 and find a median value of  $A_I = 0.075$  and  $A_I = 0.093$  mag using the [Monson et al. \(2017\)](#) and [Catelan et al. \(2004\)](#) relationships, respectively. These results well match those from the [Haschke et al. \(2011\)](#) red clump maps, but see further discussion in §5.

## 5. DISCUSSION

We sought to estimate the intrinsic color,  $(V - I)_{\text{RC},0}$ , of the red clumps of the Magellanic Clouds. Using predictions from i) the BaSTI isochrones shifted by an offset calibrated off of three stellar populations, ii) the Cepheids period-color relations, and iii) RR Lyrae period-color relations, we have estimated that  $(V - I)_{\text{RC},0,\text{LMC}} = \{0.90, 0.93, 0.93\}$  respectively, and using the first and third method that  $(V - I)_{\text{RC},0,\text{SMC}} = \{0.85, 0.88\}$  respectively. A summary of the different methods is listed in Table 4. In the pursuit of that goal, we have also demonstrated the following:

Method	$(V - I)_{RC,0,LMC}$	$(V - I)_{RC,0,SMC}$
BaSTI v1 isochrones no empirically-derived offsets	0.92	0.87
BaSTI v1 isochrones with empirically-derived offsets	0.90	0.85
<i>HST</i> -observed Cepheids assuming an empirical color-period relation	0.94	–
<i>HST</i> -observed Cepheids assuming an theoretical color-period relation	0.93	–
OGLE-observed Cepheids assuming an empirical color-period relation	0.90	–
OGLE-observed Cepheids assuming an theoretical color-period relation	0.89	–
RRab assuming a theoretical period-color relation	0.93	0.88
RRab assuming an empirical period-color relation	0.95	0.88

**Table 4.** Summary of the estimates for the intrinsic colors of the LMC and SMC red clumps from the different methods explored in this work.

1. The offset between the predictions of the BaSTI isochrones with Reimers’ mass-loss parameter  $\eta = 0.20$  and the observations of red clump stars are remarkably consistent over a broad metallicity interval. The former predicts red clump stars that are redder and brighter than the observations, by  $\Delta(V - I)_{RC,0}, \Delta M_{I,RC} \approx (0.02, 0.11)$ . That  $\Delta(V - I)_{RC,0}$  is smaller than  $\Delta M_{I,RC}$  is consistent with the finding of Salaris et al. (2016), who estimated, using the same stellar evolution code, an upper bound on the mass lost by red giant star progenitors in 47 Tuc of  $\Delta M \approx 0.17 M_{\odot}$ , some 70% larger than that predicted when assuming  $\eta = 0.20$ . The predictions of the updated BaSTI database, BaSTI version 2.0, are much more consistent with the observations, with  $\Delta(V - I)_{RC,0}, \Delta M_{I,RC} \approx (-0.01, -0.02)$ . In passing, this represents a sound evidence of the reliability and accuracy of the physical framework adopted for the new version of the BaSTI model library.
2. The different calibrations yield results that are consistent with each other. For the RR Lyrae, the widely-used theoretical period-color relation of Catelan et al. (2004) predicts LMC RR Lyrae  $(V - I)$  colors that are 0.01 mag bluer than the colors predicted by a relationship derived from the work of Monson et al. (2017). For the SMC RR Lyrae, the offset is 0.00 mag. For the LMC Cepheid sample, the theoretically-calibrated period-color relation of Fiorentino et al. (2013) agrees with the empirically-calibrated relation from Macri et al. (2006), from which the derived reddening estimates are 0.01 mag greater than those obtained using the RR Lyrae. For both of the LMC and the SMC, the reddening estimates derived from the RR Lyrae are shifted by 0.03 mag respectively with those derived from the red clump stars.

That is an impressive degree of consistency. Moreover, for the value of  $(V - I)_{RC,0}$  predicted by applying empirical shifts to the BaSTI isochrones to agree with that by assuming a match with the Cepheid-based calibration, we would only

need to increase the assumed  $[\text{Fe}/\text{H}]$  of the Large Magellanic Cloud by  $\sim 0.09$  dex. That is certainly within the margin of error. Further, our estimate of  $E(V - I)_{47\text{Tuc}}$  might also be too high by up to 0.02 mag, see the discussion in Section 2 of Salaris et al. (2016). It is also the case that reddening maps derived from observations of RR Lyrae need not perfectly agree with reddening maps derived from observations of red clump stars – the former are a more metal-poor population, and thus likely kinematically hotter. They may have a different spatial distribution with respect to the dust.

One calibration which is not consistent with those used in this work is that used by Górski et al. (2020). They estimated the reddening along different sightlines using the blue supergiant sample of Urbaneja et al. (2017) as standard crayons. A plausible explanation for this is that the blue supergiants with ages of  $\sim 1$  Myr are along sightlines with extinction greater than the mean value probed by the  $\sim 3$  arcminute, corresponding to approximately 44 parsecs, resolution of the reddening maps of Górski et al. (2020). Indeed, the mean value of  $R_V = A_V/E(B - V)$  toward the blue supergiants is  $\langle R_V \rangle = 4.5$ . That is not consistent with the standard value of  $R_V = 3.1$ . If, for example, the reddening toward the blue supergiants is due to two components of extinction, one with  $R_V = 3.1$  and another with  $R_V = 6$ , then the  $R_V = 3.1$  component, which is the only component that contributes to the red clump stars, accounts for approximately half of the extinction to the blue supergiants. Further, given that the mean error on  $R_V$  is also approximately equal to the standard deviation in the derived  $R_V$  values, it may be that all of the blue supergiants in the sample have this extra extinction along their line of sight.

Similarly, the fact that the reddening estimates toward Cepheids are consistent with those toward red clump stars and RR Lyrae indicates that there is null or negligible extra extinction toward Cepheids. Whatever extra extinction is likely to exist toward younger stars of  $t \sim 1$  Myr, it is significantly reduced or eliminated by the time those stars are  $\sim 100$  Myr old, the typical age of Cepheids (Bono et al. 2005). Because cluster disruption times are generally longer than Blue supergiant ages, it is reasonable to assume addi-

tional extinction for blue supergiants comes from their birth sites.

Skowron et al. (2020) derived reddening maps for the Magellanic Clouds based on an intrinsic RC color of  $(V-I)_0=0.876 \pm 0.013$  (LMC) and  $0.856 \pm 0.016$  derived by dereddening RC star colors in the outskirts of the Clouds (3-9 and 1-4 degrees away for the LMC and SMC, respectively) where the SFD maps should give more valid results. While these values are 0.02 (LMC) and 0.01 (SMC) mag bluer in V-I than what was derived here from the calibrated isochrones, this difference can be easily understood as resulting from the difference in metallicity where each result was derived. The isochrones and our empirical calibration show a 0.02 mag increase in V-I color for an 0.1 dex increase in metallicity (Equations 1 and 3). The Skowron et al. (2020) derived color would thus match ours for a metallicity in the Clouds's outskirts which is lower by 0.1 dex than the mean of the bar and disk stars used here. Indeed, an ideal approach towards reddening maps derived from RC stars would include the effect of the metallicity gradient on the RC star color using the calibrated isochrones and would be expected to match the Haschke et al. (2011) maps in the higher density regions of the Clouds and the Skowron et al. (2020) maps in the outskirts.

Freedman et al. (2020) present a method to measure the reddening of TRGB stars in the LMC that does not appear to agree with the LMC reddening maps previously discussed. They simultaneously measured the difference in distance and reddening between the LMC and another host using the colors of their respective TRGBs, e.g., in the SMC and LMC:

$$\Delta\mu(\text{SMC} - \text{LMC}) = (m_{x,\text{SMC}} - R(x, I)A_{I,\text{SMC}}) - (m_{x,\text{LMC}} - R(x, I)A_{I,\text{LMC}}). \quad (10)$$

where  $m_{x,\text{SMC}}$  is the apparent magnitude of TRGB in one of 5 bands ( $V, I, J, H, K_s$ ), and  $R(x, I)$  is the ratio of extinction between band  $x$  and  $I$ . They estimate  $A_{I,\text{SMC}}$  from the Galactic foreground reddening maps of Schlafly & Finkbeiner (2011) as given in NED, then solve for two parameters,  $\Delta\mu$  and  $A_{I,\text{LMC}}$ . They find a significantly higher value of  $A_I = 0.169 \pm 0.02$ ,  $> 3 \sigma$  higher than the value derived from the red clump star map of Haschke et al. (2011) or the RR Lyae maps presented here and a more luminous calibration of  $M_I$  for TRGB by 0.08 mag, a direct consequence of the enhanced extinction. However, an apparent discrepancy in measurements of the TRGB  $m_{I,\text{SMC}}$  might explain this difference.

Freedman et al. (2020) report a value of SMC TRGB  $m_{I,\text{SMC}} = 14.93 \pm 0.01$  from OGLE photometry. Górski et al. (2016) found the SMC TRGB from OGLE photometry is broad and brighter and varies across five SMC fields from 14.98 to 15.20 with a mean of  $m_I = 15.04$ . Yuan et al. (2019) found  $m_I = 15.01$  from the OGLE data, consis-

tent with Górski et al. (2016) but also brighter than Freedman et al. (2020) by  $\sim 0.1$  mag. As shown in equation 10,  $m_{I,\text{SMC}} + A_{I,\text{LMC}} \sim \Delta\mu$  so a higher value of  $m_{I,\text{SMC}}$  by  $\sim 0.1$  mag than Freedman et al. (2020) yields a lower value of  $A_{I,\text{LMC}}$  by this difference for the same  $\Delta\mu$  ( $\Delta\mu$  is well constrained in the measured range by the relative detached eclipsing binary distance from Wielgórski et al. (2017) with  $\sigma = 0.026$  mag) and could explain the discrepancy with the LMC reddening maps. Freedman et al. (2020) does not indicate which stars in the SMC (or LMC) OGLE catalogues (*i.e.*, the region, mag range or filtering characteristics) were employed to measure the TRGB so we cannot readily resolve or reproduce the differences in  $m_{I,\text{SMC}}$  with Górski et al. (2016) or Yuan et al. (2019).

Another source of discrepancy is the foreground estimate of  $A_{I,\text{SMC}}$  used by Freedman et al. (2020) via NED. This value is quite uncertain because it can not be derived *directly* from the the IRAS maps (Neugebauer et al. 1984) used by Schlafly & Finkbeiner (2011) because the Magellanic Clouds contaminate the foreground glow. One may interpolate the IRAS maps around the  $\sim 10$  degree perimeter of the SMC where the maps show  $\sigma \sim E(B - V) \sim 0.015$  mag (the Magellanic Stream also provides regional contamination of the IRAS maps) resulting in an uncertainty of  $A_{V,\text{SMC}}$  of 0.05 mag which lowers the precision of the TRGB method considerably. In addition, the large range in the SMC TRGB values may result from a large depth (Subramanian & Subramanian 2012) which also challenges the precision of the SMC to LMC comparison. An independent comparison between the LMC and IC 1613 (old, dwarf elliptical) by Freedman et al. (2020) avoids the issues with the SMC but the metallicities and ages of the TRGB span a larger range of one dex and systematic differences in TRGB may arise. Freedman et al. (2020) accounts for age and metallicity differences with a linear color term, but there is empirical evidence that this may not fully rectify the disparity; there is excessive dispersion beyond the quoted 0.01 mag TRGB errors between hosts as the  $\chi^2$  for the color comparison (equation (10) for the LMC-IC 1613 comparison) is 16 for 3 degrees of freedom ( $P=0.1\%$ ). Whether the high value of  $\chi^2$  is due to higher measurement errors or intrinsic variation in color-corrected TRGB colors (see McQuinn et al. (2019)), the uncertainty in  $A_{I,\text{LMC}}$  would be higher by  $\sim \sqrt{5}$ .

Could the sight lines of TRGB in the LMC have much higher extinction than red clump or RR Lyae tracers? In principle, red clump and RR Lyae stars should provide good measures of dust sight lines for near-TRGB stars as they are all highly evolved red giants of  $\geq$  Gyr timescales. In general, older populations have more time to migrate from their dusty star-forming birth sites so a hierarchy of ages would correspond to a hierarchy of extinction. As shown in Sections 4.1 and 4.2 the red clump star maps of Haschke et al. (2011) agree

with the colors of Cepheids which are even younger (at 50-100 Myr) than the red clump stars. TRGB stars should be a slightly older population (an older stellar population produces fewer horizontal branch and particularly fewer red clump stars per capita, and correspondingly, more red giant stars) so it is unlikely TRGB stars would have statistically more extinction than red clump stars and Cepheids. Freedman et al. (2020) and Joshi & Panchal (2019) identify a range of recent LMC literature values of  $A_I$  of 0.10 to 0.20 mag measured from B Stars, red clump Stars, RR Lyrae, star clusters, Cepheids and detached eclipsing binary stars. The Freedman et al. (2020) value of  $A_I=0.17$  mag falls at the higher end of this range and the value of  $A_I=0.10$  mag from the Haschke et al. (2011) maps at the lower end. Because all of these stellar tracers are younger and likely along dustier sightlines than TRGB stars (with the exception of RR Lyrae), considering the range and age of the population, TRGB stars would seem likely to fall at the low end of this range.

An attractive alternative to estimating the extinction of TRGB in the LMC is to calibrate it in the halo of the maser host NGC 4258 (Jang & Lee 2017a; Reid, Pesce, & Riess 2019) where the result, like the application in SN Ia hosts, is insensitive to dust.

### 5.1. Prospects for Further Work

Additional and independent estimates of the reddening toward the Magellanic Clouds would be useful not just to simply further calibrate the latter, but alternatively, to explore the consistency of different approaches. Among the possibilities:

1. To compare the predictions for the red clump of the BaSTI isochrones, either of version 1 or version 2, with a larger sample robust empirical anchors. We would have liked to do so, but most of the metal-rich clusters are toward the inner Milky Way and thus have non-standard extinction along their lines of sight (Nishiyama et al. 2008; Nataf et al. 2016). Separately, the horizontal branch morphologies of globular clusters are sensitive to variations in the initial abundances of helium (Busso et al. 2007; Dotter et al. 2010; Milone et al. 2014; Marino et al. 2014). The latter are not always as well determined as they are for 47 Tuc.
2. To measure the foreground reddening toward the Magellanic Clouds using both a probabilistic analysis of the spectroscopic, photometric, and parallax information of foreground stars in GALAH (De Silva et al. 2015), as well as the measurements of the equivalent widths of the diffuse interstellar bands in their spectra. We could not do so here as the reddening estimates are not in the most up-to-date publicly-available data release (Buder et al. 2019). We did attempt to do this with APOGEE data, from which we estimated the fore-

ground  $A_I \approx 0.12$ , but that sample was of only  $\sim 30$  stars.

3. To measure additional colors of the red clump, to break the degeneracy between reddening variations and intrinsic color variations. We attempted to do this with the  $(g-i)$  measurements of Choi et al. (2018), but this did not yield a robust constraint as  $E(g-i)/E(V-I)$  has approximately the same value as the  $\delta(g-i)/\delta(V-I)$  that results from variations in stellar effective temperature. In contrast, with infra-red data,  $E(I-K_s)/E(V-I) \approx 1.04$ , and  $\delta(I-K_s)/\delta(V-I) \approx 0.47$ .
4. To use open and globular clusters in the Magellanic Clouds as standard crayons. At this time, that literature is very heterogeneous in its assumptions (choice of isochrones, rotation rates, etc) and thus the resultant reddening scale ends up being subjective. Further, many of the clusters have photometric metallicity estimates, for which the derivation is degenerate with that of the reddening.
5. To obtain spectroscopic  $[\text{Fe}/\text{H}]$  and hopefully  $[\alpha/\text{Fe}]$  measurements for a larger number of solar neighbourhood RR Lyrae.

## 6. CONCLUSION

In this investigation we have investigated three different methods to estimate the intrinsic color,  $(V-I)_{RC,0}$  of the red clumps of the Magellanic Clouds.

The first method was derived from the predictions of the BaSTI version 1 isochrones, for which we applied empirically-calibrated offsets calibrated by comparing the isochrone predictions to the observations of the globular cluster 47 Tuc, the solar neighbourhood, and the open cluster NGC 6791. Together, these three populations constitute a robust calibration set, as they span a metallicity range of  $\Delta[\text{Fe}/\text{H}] \approx 1.1$  dex. The BaSTI isochrones predict red clumps that are slightly red and bright relative to the observations, by  $\Delta(V-I)_{RC,0}$ ,  $\Delta M_{I,RC} \approx (0.02, 0.11)$ . We note that these offsets are almost equal to the offsets between the BaSTI version 1 and version 2 isochrones. We applied this offset to calculate our first estimate of the red clumps of the Magellanic Clouds, and obtained  $(V-I)_{RC,0,LMC} = 0.90$  and  $(V-I)_{RC,0,SMC} = 0.85$ , and also  $M_{I,RC,LMC} \approx -0.31$  and  $M_{I,RC,SMC} \approx -0.39$ .

The second method derived estimates by comparing the reddening toward Cepheids, for which we assumed that the average intrinsic colors can be reliably determined from period-color relations, with the reddening values estimated from the nearest red clump centroid measurement. The estimate was nearly the same regardless of whether or not we used the empirically-calibrated period-color relation of Macri

et al. (2006) or the theoretically-derived period-color relation of Fiorentino et al. (2013). The resulting estimate was  $(V - I)_{RC,0,LMC} = 0.93$ .

The third method derived estimates by using the OGLE RR Lyrae catalogue of Soszyński et al. (2016) as a set of standard crayons with which to estimate the reddening along their lines of sight. The  $(V - I)_{RRab}$  colors predicted by the theoretically-derived period-color relation of Catelan et al. (2004), and one empirically calibrated from the data of Monson et al. (2017) agree to 0.01 mag or better. Using the second relation, we estimated  $(V - I)_{RC,0,LMC} = 0.93$  and  $(V - I)_{RC,0,SMC} = 0.88$ .

#### ACKNOWLEDGMENTS

We thank Aaron Dotter, Adriano Pietrinferni, and Dan Scolnic for helpful discussion.

DMN acknowledges support from NASA under award Number 80NSSC19K0589, and support from the Allan C. And Dorothy H. Davis Fellowship. SC acknowledges support from Premiale INAF MITIC, from Istituto Nazionale di Fisica Nucleare (INFN) (Iniziativa specifica TAsP), and grant AYA2013- 42781P from the Ministry of Economy and Competitiveness of Spain. LC acknowledges support from the Australian Research Council Future Fellowship FT160100402.

This work has made use of data from the European Space Agency (ESA) mission *Gaia* (<https://www.cosmos.esa.int/gaia>), processed by the *Gaia* Data Processing and Analysis Consortium (DPAC, <https://www.cosmos.esa.int/web/gaia/dpac/consortium>). Funding for the DPAC has been provided by national institutions, in particular the institutions participating in the *Gaia* Multilateral Agreement.

This publication makes use of data products from the Two Micron All Sky Survey, which is a joint project of the Univer-

sity of Massachusetts and the Infrared Processing and Analysis Center/California Institute of Technology, funded by the National Aeronautics and Space Administration and the National Science Foundation.

Funding for the Sloan Digital Sky Survey IV has been provided by the Alfred P. Sloan Foundation, the U.S. Department of Energy Office of Science, and the Participating Institutions. SDSS-IV acknowledges support and resources from the Center for High-Performance Computing at the University of Utah. The SDSS web site is [www.sdss.org](http://www.sdss.org).

SDSS-IV is managed by the Astrophysical Research Consortium for the Participating Institutions of the SDSS Collaboration including the Brazilian Participation Group, the Carnegie Institution for Science, Carnegie Mellon University, the Chilean Participation Group, the French Participation Group, Harvard-Smithsonian Center for Astrophysics, Instituto de Astrofísica de Canarias, The Johns Hopkins University, Kavli Institute for the Physics and Mathematics of the Universe (IPMU) / University of Tokyo, the Korean Participation Group, Lawrence Berkeley National Laboratory, Leibniz Institut für Astrophysik Potsdam (AIP), Max-Planck-Institut für Astronomie (MPIA Heidelberg), Max-Planck-Institut für Astrophysik (MPA Garching), Max-Planck-Institut für Extraterrestrische Physik (MPE), National Astronomical Observatories of China, New Mexico State University, New York University, University of Notre Dame, Observatório Nacional / MCTI, The Ohio State University, Pennsylvania State University, Shanghai Astronomical Observatory, United Kingdom Participation Group, Universidad Nacional Autónoma de México, University of Arizona, University of Colorado Boulder, University of Oxford, University of Portsmouth, University of Utah, University of Virginia, University of Washington, University of Wisconsin, Vanderbilt University, and Yale University.

#### REFERENCES

- An, D., Terndrup, D. M., Pinsonneault, M. H., & Lee, J.-W. 2015, *ApJ*, 811, 46, doi: [10.1088/0004-637X/811/1/46](https://doi.org/10.1088/0004-637X/811/1/46)
- Anthony-Twarog, B. J., Twarog, B. A., & Mayer, L. 2007, *AJ*, 133, 1585, doi: [10.1086/511976](https://doi.org/10.1086/511976)
- Bailer-Jones, C. A. L., Rybizki, J., Fousneau, M., Mantelet, G., & Andrae, R. 2018, *AJ*, 156, 58, doi: [10.3847/1538-3881/aacb21](https://doi.org/10.3847/1538-3881/aacb21)
- Baumgardt, H., Hilker, M., Sollima, A., & Bellini, A. 2019, *MNRAS*, 482, 5138, doi: [10.1093/mnras/sty2997](https://doi.org/10.1093/mnras/sty2997)
- Bergbusch, P. A., & Stetson, P. B. 2009, *AJ*, 138, 1455, doi: [10.1088/0004-6256/138/5/1455](https://doi.org/10.1088/0004-6256/138/5/1455)
- Blanton, M. R., Bershady, M. A., Abolfathi, B., et al. 2017, *AJ*, 154, 28, doi: [10.3847/1538-3881/aa7567](https://doi.org/10.3847/1538-3881/aa7567)
- Boesgaard, A. M., Lum, M. G., & Deliyannis, C. P. 2015, *ApJ*, 799, 202, doi: [10.1088/0004-637X/799/2/202](https://doi.org/10.1088/0004-637X/799/2/202)
- Bono, G., Marconi, M., Cassisi, S., et al. 2005, *ApJ*, 621, 966, doi: [10.1086/427744](https://doi.org/10.1086/427744)
- Bovy, J., Nidever, D. L., Rix, H.-W., et al. 2014, *ApJ*, 790, 127, doi: [10.1088/0004-637X/790/2/127](https://doi.org/10.1088/0004-637X/790/2/127)
- Brogaard, K., VandenBerg, D. A., Bruntt, H., et al. 2012, *A&A*, 543, A106, doi: [10.1051/0004-6361/201219196](https://doi.org/10.1051/0004-6361/201219196)
- Buder, S., Lind, K., Ness, M. K., et al. 2019, *A&A*, 624, A19, doi: [10.1051/0004-6361/201833218](https://doi.org/10.1051/0004-6361/201833218)
- Busso, G., Cassisi, S., Piotto, G., et al. 2007, *A&A*, 474, 105, doi: [10.1051/0004-6361:20077806](https://doi.org/10.1051/0004-6361:20077806)
- Caffau, E., Ludwig, H. G., Steffen, M., Freytag, B., & Bonifacio, P. 2011, *SoPh*, 268, 255, doi: [10.1007/s11207-010-9541-4](https://doi.org/10.1007/s11207-010-9541-4)
- Carrell, K., Wilhelm, R., & Chen, Y. 2012, *AJ*, 144, 18, doi: [10.1088/0004-6256/144/1/18](https://doi.org/10.1088/0004-6256/144/1/18)

- Casagrande, L., & VandenBerg, D. A. 2014, *MNRAS*, 444, 392, doi: [10.1093/mnras/stu1476](https://doi.org/10.1093/mnras/stu1476)
- Cassisi, S., Castellani, M., Caputo, F., & Castellani, V. 2004, *A&A*, 426, 641, doi: [10.1051/0004-6361:20041048](https://doi.org/10.1051/0004-6361:20041048)
- Cassisi, S., Potekhin, A. Y., Pietrinferni, A., Catelan, M., & Salaris, M. 2007, *ApJ*, 661, 1094, doi: [10.1086/516819](https://doi.org/10.1086/516819)
- Catelan, M., Pritzl, B. J., & Smith, H. A. 2004, *ApJS*, 154, 633, doi: [10.1086/422916](https://doi.org/10.1086/422916)
- Chan, V. C., & Bovy, J. 2019, arXiv e-prints, arXiv:1910.00398. <https://arxiv.org/abs/1910.00398>
- Chen, Y. Q., Casagrande, L., Zhao, G., et al. 2017, *ApJ*, 840, 77, doi: [10.3847/1538-4357/aa6d0f](https://doi.org/10.3847/1538-4357/aa6d0f)
- Choi, Y., Nidever, D. L., Olsen, K., et al. 2018, *ApJ*, 866, 90, doi: [10.3847/1538-4357/aae083](https://doi.org/10.3847/1538-4357/aae083)
- Cohen, R. E., Kalirai, J. S., Gilbert, K. M., et al. 2018, *AJ*, 156, 230, doi: [10.3847/1538-3881/aae52d](https://doi.org/10.3847/1538-3881/aae52d)
- Cole, A. A. 1998, *ApJL*, 500, L137, doi: [10.1086/311422](https://doi.org/10.1086/311422)
- Cordier, D., Pietrinferni, A., Cassisi, S., & Salaris, M. 2007, *AJ*, 133, 468, doi: [10.1086/509870](https://doi.org/10.1086/509870)
- Correnti, M., Bellazzini, M., Ibata, R. A., Ferraro, F. R., & Varghese, A. 2010, *ApJ*, 721, 329, doi: [10.1088/0004-637X/721/1/329](https://doi.org/10.1088/0004-637X/721/1/329)
- De Silva, G. M., Freeman, K. C., Bland-Hawthorn, J., et al. 2015, *MNRAS*, 449, 2604, doi: [10.1093/mnras/stv327](https://doi.org/10.1093/mnras/stv327)
- di Criscienzo, M., Ventura, P., D'Antona, F., Milone, A., & Piotto, G. 2010, *MNRAS*, 408, 999, doi: [10.1111/j.1365-2966.2010.17168.x](https://doi.org/10.1111/j.1365-2966.2010.17168.x)
- Dolphin, A. E. 2002, *MNRAS*, 332, 91, doi: [10.1046/j.1365-8711.2002.05271.x](https://doi.org/10.1046/j.1365-8711.2002.05271.x)
- Donor, J., Frinchaboy, P. M., Cunha, K., et al. 2018, *AJ*, 156, 142, doi: [10.3847/1538-3881/aad635](https://doi.org/10.3847/1538-3881/aad635)
- Dotter, A., Sarajedini, A., Anderson, J., et al. 2010, *ApJ*, 708, 698, doi: [10.1088/0004-637X/708/1/698](https://doi.org/10.1088/0004-637X/708/1/698)
- Ferguson, J. W., Alexander, D. R., Allard, F., et al. 2005, *ApJ*, 623, 585, doi: [10.1086/428642](https://doi.org/10.1086/428642)
- Fernley, J., & Barnes, T. G. 1997, *A&AS*, 125, 313, doi: [10.1051/aas:1997222](https://doi.org/10.1051/aas:1997222)
- Feuillet, D. K., Frankel, N., Lind, K., et al. 2019, *MNRAS*, 489, 1742, doi: [10.1093/mnras/stz2221](https://doi.org/10.1093/mnras/stz2221)
- Fiorentino, G., Musella, I., & Marconi, M. 2013, *MNRAS*, 434, 2866, doi: [10.1093/mnras/stt1193](https://doi.org/10.1093/mnras/stt1193)
- Fitzpatrick, E. L. 1999, *PASP*, 111, 63, doi: [10.1086/316293](https://doi.org/10.1086/316293)
- Flewelling, H. A., Magnier, E. A., Chambers, K. C., et al. 2016, arXiv e-prints, arXiv:1612.05243. <https://arxiv.org/abs/1612.05243>
- Freedman, W. L., Madore, B. F., Hoyt, T., et al. 2020, *ApJ*, 891, 57, doi: [10.3847/1538-4357/ab7339](https://doi.org/10.3847/1538-4357/ab7339)
- Gaia Collaboration, Prusti, T., de Bruijne, J. H. J., et al. 2016, *A&A*, 595, A1, doi: [10.1051/0004-6361/201629272](https://doi.org/10.1051/0004-6361/201629272)
- García-Berro, E., Torres, S., Althaus, L. r. G., et al. 2010, *Nature*, 465, 194, doi: [10.1038/nature09045](https://doi.org/10.1038/nature09045)
- García Pérez, A. E., Allende Prieto, C., Holtzman, J. A., et al. 2016, *AJ*, 151, 144, doi: [10.3847/0004-6256/151/6/144](https://doi.org/10.3847/0004-6256/151/6/144)
- Gilmozzi, R., & Spyromilio, J. 2007, *The Messenger*, 127, 11
- Girardi, L., & Salaris, M. 2001, *MNRAS*, 323, 109, doi: [10.1046/j.1365-8711.2001.04084.x](https://doi.org/10.1046/j.1365-8711.2001.04084.x)
- Górski, M., Pietrzyński, G., Gieren, W., et al. 2016, *AJ*, 151, 167, doi: [10.3847/0004-6256/151/6/167](https://doi.org/10.3847/0004-6256/151/6/167)
- Górski, M., Zgierski, B., Pietrzyński, G., et al. 2020, *ApJ*, 889, 179, doi: [10.3847/1538-4357/ab65ed](https://doi.org/10.3847/1538-4357/ab65ed)
- Graczyk, D., Pietrzyński, G., Thompson, I. B., et al. 2014, *ApJ*, 780, 59, doi: [10.1088/0004-637X/780/1/59](https://doi.org/10.1088/0004-637X/780/1/59)
- Gratton, R. G., Lucatello, S., Sollima, A., et al. 2013, *A&A*, 549, A41, doi: [10.1051/0004-6361/201219976](https://doi.org/10.1051/0004-6361/201219976)
- Green, G. M., Schlafly, E., Zucker, C., Speagle, J. S., & Finkbeiner, D. 2019, *ApJ*, 887, 93, doi: [10.3847/1538-4357/ab5362](https://doi.org/10.3847/1538-4357/ab5362)
- Grundahl, F., Stetson, P. B., & Andersen, M. I. 2002, *A&A*, 395, 481, doi: [10.1051/0004-6361:20020790](https://doi.org/10.1051/0004-6361:20020790)
- Hansen, B. M. S., Kalirai, J. S., Anderson, J., et al. 2013, *Nature*, 500, 51, doi: [10.1038/nature12334](https://doi.org/10.1038/nature12334)
- Haschke, R., Grebel, E. K., & Duffau, S. 2011, *AJ*, 141, 158, doi: [10.1088/0004-6256/141/5/158](https://doi.org/10.1088/0004-6256/141/5/158)
- Hawkins, K., Leistedt, B., Bovy, J., & Hogg, D. W. 2017, *MNRAS*, 471, 722, doi: [10.1093/mnras/stx1655](https://doi.org/10.1093/mnras/stx1655)
- Hidalgo, S. L., Pietrinferni, A., Cassisi, S., et al. 2018, *ApJ*, 856, 125, doi: [10.3847/1538-4357/aab158](https://doi.org/10.3847/1538-4357/aab158)
- Inno, L., Bono, G., Matsunaga, N., et al. 2016, *ApJ*, 832, 176, doi: [10.3847/0004-637X/832/2/176](https://doi.org/10.3847/0004-637X/832/2/176)
- Jang, I. S., & Lee, M. G. 2017a, *ApJ*, 835, 28, doi: [10.3847/1538-4357/835/1/28](https://doi.org/10.3847/1538-4357/835/1/28)
- . 2017b, *ApJ*, 836, 74, doi: [10.3847/1538-4357/836/1/74](https://doi.org/10.3847/1538-4357/836/1/74)
- Johnson, C. I., McDonald, I., Pilachowski, C. A., et al. 2015, *AJ*, 149, 71, doi: [10.1088/0004-6256/149/2/71](https://doi.org/10.1088/0004-6256/149/2/71)
- Jönsson, H., Allende Prieto, C., Holtzman, J. A., et al. 2018, *AJ*, 156, 126, doi: [10.3847/1538-3881/aad4f5](https://doi.org/10.3847/1538-3881/aad4f5)
- Joshi, Y. C., & Panchal, A. 2019, *A&A*, 628, A51, doi: [10.1051/0004-6361/201834574](https://doi.org/10.1051/0004-6361/201834574)
- Kunder, A., Rich, R. M., Koch, A., et al. 2016, *ApJL*, 821, L25, doi: [10.3847/2041-8205/821/2/L25](https://doi.org/10.3847/2041-8205/821/2/L25)
- Lee, Y.-W., Demarque, P., & Zinn, R. 1994, *ApJ*, 423, 248, doi: [10.1086/173803](https://doi.org/10.1086/173803)
- Lindegren, L., Hernández, J., Bombrun, A., et al. 2018, *A&A*, 616, A2, doi: [10.1051/0004-6361/201832727](https://doi.org/10.1051/0004-6361/201832727)
- Macri, L. M., Ngeow, C.-C., Kanbur, S. M., Mahzooni, S., & Smitka, M. T. 2015, *AJ*, 149, 117, doi: [10.1088/0004-6256/149/4/117](https://doi.org/10.1088/0004-6256/149/4/117)
- Macri, L. M., Stanek, K. Z., Bersier, D., Greenhill, L. J., & Reid, M. J. 2006, *ApJ*, 652, 1133, doi: [10.1086/508530](https://doi.org/10.1086/508530)

- Majewski, S. R., Schiavon, R. P., Frinchaboy, P. M., et al. 2017, *AJ*, 154, 94, doi: [10.3847/1538-3881/aa784d](https://doi.org/10.3847/1538-3881/aa784d)
- Marino, A. F., Milone, A. P., Przybilla, N., et al. 2014, *MNRAS*, 437, 1609, doi: [10.1093/mnras/stt1993](https://doi.org/10.1093/mnras/stt1993)
- Marino, A. F., Milone, A. P., Casagrande, L., et al. 2016, *MNRAS*, 459, 610, doi: [10.1093/mnras/stw611](https://doi.org/10.1093/mnras/stw611)
- McKeever, J. M., Basu, S., & Corsaro, E. 2019, *ApJ*, 874, 180, doi: [10.3847/1538-4357/ab0c04](https://doi.org/10.3847/1538-4357/ab0c04)
- McQuinn, K. B. W., Boyer, M., Skillman, E. D., & Dolphin, A. E. 2019, *ApJ*, 880, 63, doi: [10.3847/1538-4357/ab2627](https://doi.org/10.3847/1538-4357/ab2627)
- McWilliam, A., & Zoccali, M. 2010, *ApJ*, 724, 1491, doi: [10.1088/0004-637X/724/2/1491](https://doi.org/10.1088/0004-637X/724/2/1491)
- Miglio, A., Brogaard, K., Stello, D., et al. 2012, *MNRAS*, 419, 2077, doi: [10.1111/j.1365-2966.2011.19859.x](https://doi.org/10.1111/j.1365-2966.2011.19859.x)
- Milone, A. P., Piotto, G., Bedin, L. R., et al. 2012, *ApJ*, 744, 58, doi: [10.1088/0004-637X/744/1/58](https://doi.org/10.1088/0004-637X/744/1/58)
- Milone, A. P., Marino, A. F., Dotter, A., et al. 2014, *ApJ*, 785, 21, doi: [10.1088/0004-637X/785/1/21](https://doi.org/10.1088/0004-637X/785/1/21)
- Milone, A. P., Piotto, G., Renzini, A., et al. 2017, *MNRAS*, 464, 3636, doi: [10.1093/mnras/stw2531](https://doi.org/10.1093/mnras/stw2531)
- Milone, A. P., Marino, A. F., Renzini, A., et al. 2018, *MNRAS*, 481, 5098, doi: [10.1093/mnras/sty2573](https://doi.org/10.1093/mnras/sty2573)
- Monson, A. J., Beaton, R. L., Scowcroft, V., et al. 2017, *AJ*, 153, 96, doi: [10.3847/1538-3881/153/3/96](https://doi.org/10.3847/1538-3881/153/3/96)
- Mould, J., Clementini, G., & Da Costa, G. 2019, *PASA*, 36, e001, doi: [10.1017/pasa.2018.46](https://doi.org/10.1017/pasa.2018.46)
- Mucciarelli, A. 2014, *Astronomische Nachrichten*, 335, 79, doi: [10.1002/asna.201312006](https://doi.org/10.1002/asna.201312006)
- Nataf, D. M., Cassisi, S., & Athanassoula, E. 2014, *MNRAS*, 442, 2075, doi: [10.1093/mnras/stu805](https://doi.org/10.1093/mnras/stu805)
- Nataf, D. M., Gould, A., Pinsonneault, M. H., & Stetson, P. B. 2011, *ApJ*, 736, 94, doi: [10.1088/0004-637X/736/2/94](https://doi.org/10.1088/0004-637X/736/2/94)
- Nataf, D. M., Udalski, A., Gould, A., Fouqué, P., & Stanek, K. Z. 2010, *ApJL*, 721, L28, doi: [10.1088/2041-8205/721/1/L28](https://doi.org/10.1088/2041-8205/721/1/L28)
- Nataf, D. M., Gonzalez, O. A., Casagrande, L., et al. 2016, *MNRAS*, 456, 2692, doi: [10.1093/mnras/stv2843](https://doi.org/10.1093/mnras/stv2843)
- Nataf, D. M., Wyse, R. F. G., Schiavon, R. P., et al. 2019, *AJ*, 158, 14, doi: [10.3847/1538-3881/ab1a27](https://doi.org/10.3847/1538-3881/ab1a27)
- Neugebauer, G., Habing, H. J., van Duinen, R., et al. 1984, *ApJL*, 278, L1, doi: [10.1086/184209](https://doi.org/10.1086/184209)
- Nidever, D. L., Bovy, J., Bird, J. C., et al. 2014, *ApJ*, 796, 38, doi: [10.1088/0004-637X/796/1/38](https://doi.org/10.1088/0004-637X/796/1/38)
- Nidever, D. L., Hasselquist, S., Hayes, C. R., et al. 2019, arXiv e-prints, arXiv:1901.03448. <https://arxiv.org/abs/1901.03448>
- Nishiyama, S., Nagata, T., Tamura, M., et al. 2008, *ApJ*, 680, 1174, doi: [10.1086/587791](https://doi.org/10.1086/587791)
- Nogueras-Lara, F., Schödel, R., Gallego-Calvente, A. T., et al. 2019, *Nature Astronomy*, doi: [10.1038/s41550-019-0967-9](https://doi.org/10.1038/s41550-019-0967-9)
- Paczynski, B., & Stanek, K. Z. 1998, *ApJL*, 494, L219, doi: [10.1086/311181](https://doi.org/10.1086/311181)
- Parisi, M. C., Geisler, D., Carraro, G., et al. 2016, *AJ*, 152, 58, doi: [10.3847/0004-6256/152/3/58](https://doi.org/10.3847/0004-6256/152/3/58)
- Percival, S. M., & Salaris, M. 2003, *MNRAS*, 343, 539, doi: [10.1046/j.1365-8711.2003.06691.x](https://doi.org/10.1046/j.1365-8711.2003.06691.x)
- Perryman, M. A. C., Lindegren, L., Kovalevsky, J., et al. 1997, *A&A*, 500, 501
- Pietrinferni, A., Cassisi, S., & Salaris, M. 2010, *A&A*, 522, A76, doi: [10.1051/0004-6361/201015065](https://doi.org/10.1051/0004-6361/201015065)
- Pietrinferni, A., Cassisi, S., Salaris, M., & Castelli, F. 2004, *ApJ*, 612, 168, doi: [10.1086/422498](https://doi.org/10.1086/422498)
- . 2006, *ApJ*, 642, 797, doi: [10.1086/501344](https://doi.org/10.1086/501344)
- Pietrukowicz, P., Kozłowski, S., Skowron, J., et al. 2015, *ApJ*, 811, 113, doi: [10.1088/0004-637X/811/2/113](https://doi.org/10.1088/0004-637X/811/2/113)
- Pietrzyński, G., Górski, M., Gieren, W., et al. 2010, *AJ*, 140, 1038, doi: [10.1088/0004-6256/140/4/1038](https://doi.org/10.1088/0004-6256/140/4/1038)
- Pietrzyński, G., Graczyk, D., Gallette, A., et al. 2019, *Nature*, 567, 200, doi: [10.1038/s41586-019-0999-4](https://doi.org/10.1038/s41586-019-0999-4)
- Reid, M. J., Pesce, D. W., & Riess, A. G. 2019, *ApJL*, 886, L27, doi: [10.3847/2041-8213/ab552d](https://doi.org/10.3847/2041-8213/ab552d)
- Reimers, D. 1975, *Memoires of the Societe Royale des Sciences de Liege*, 8, 369
- Riess, A. G., Casertano, S., Yuan, W., Macri, L. M., & Scolnic, D. 2019, *ApJ*, 876, 85, doi: [10.3847/1538-4357/ab1422](https://doi.org/10.3847/1538-4357/ab1422)
- Riess, A. G., Macri, L. M., Hoffmann, S. L., et al. 2016, *ApJ*, 826, 56, doi: [10.3847/0004-637X/826/1/56](https://doi.org/10.3847/0004-637X/826/1/56)
- Salaris, M., Cassisi, S., & Pietrinferni, A. 2016, *A&A*, 590, A64, doi: [10.1051/0004-6361/201628181](https://doi.org/10.1051/0004-6361/201628181)
- Salaris, M., & Girardi, L. 2002, *MNRAS*, 337, 332, doi: [10.1046/j.1365-8711.2002.05917.x](https://doi.org/10.1046/j.1365-8711.2002.05917.x)
- Sarajedini, A., Bedin, L. R., Chaboyer, B., et al. 2007, *AJ*, 133, 1658, doi: [10.1086/511979](https://doi.org/10.1086/511979)
- Schlafly, E. F., & Finkbeiner, D. P. 2011, *ApJ*, 737, 103, doi: [10.1088/0004-637X/737/2/103](https://doi.org/10.1088/0004-637X/737/2/103)
- Schönrich, R., McMillan, P., & Eyer, L. 2019, *MNRAS*, 487, 3568, doi: [10.1093/mnras/stz1451](https://doi.org/10.1093/mnras/stz1451)
- Skowron, D. M., Skowron, J., Udalski, A., et al. 2020, arXiv e-prints, arXiv:2006.02448. <https://arxiv.org/abs/2006.02448>
- Skrutskie, M. F., Cutri, R. M., Stiening, R., et al. 2006, *AJ*, 131, 1163, doi: [10.1086/498708](https://doi.org/10.1086/498708)
- Smolec, R. 2005, *AcA*, 55, 59. <https://arxiv.org/abs/astro-ph/0503614>
- Soszyński, I., Udalski, A., Szymański, M. K., et al. 2016, *AcA*, 66, 131. <https://arxiv.org/abs/1606.02727>
- Stanek, K. Z., & Garnavich, P. M. 1998, *ApJL*, 503, L131, doi: [10.1086/311539](https://doi.org/10.1086/311539)
- Stanek, K. Z., Udalski, A., Szymański, M., et al. 1997, *ApJ*, 477, 163, doi: [10.1086/303702](https://doi.org/10.1086/303702)
- Stetson, P. B., Bruntt, H., & Grundahl, F. 2003, *PASP*, 115, 413, doi: [10.1086/368337](https://doi.org/10.1086/368337)

- Subramanian, S., & Subramaniam, A. 2012, *ApJ*, 744, 128, doi: [10.1088/0004-637X/744/2/128](https://doi.org/10.1088/0004-637X/744/2/128)
- Thompson, I. B., Udalski, A., Dotter, A., et al. 2020, *MNRAS*, 492, 4254, doi: [10.1093/mnras/staa032](https://doi.org/10.1093/mnras/staa032)
- Thygesen, A. O., Sbordone, L., Andrievsky, S., et al. 2014, *A&A*, 572, A108, doi: [10.1051/0004-6361/201424533](https://doi.org/10.1051/0004-6361/201424533)
- Udalski, A., Szymanski, M., Kubiak, M., et al. 1998, *AcA*, 48, 1. <https://arxiv.org/abs/astro-ph/9803035>
- Udalski, A., Szymański, M. K., & Szymański, G. 2015, *AcA*, 65, 1. <https://arxiv.org/abs/1504.05966>
- Udalski, A., Soszynski, I., Szymanski, M. K., et al. 2008a, *AcA*, 58, 89. <https://arxiv.org/abs/0807.3889>
- Udalski, A., Soszyński, I., Szymański, M. K., et al. 2008b, *AcA*, 58, 329. <https://arxiv.org/abs/0901.4632>
- Urbaneja, M. A., Kudritzki, R. P., Gieren, W., et al. 2017, *AJ*, 154, 102, doi: [10.3847/1538-3881/aa79a8](https://doi.org/10.3847/1538-3881/aa79a8)
- Van der Swaelmen, M., Hill, V., Primas, F., & Cole, A. A. 2013, *A&A*, 560, A44, doi: [10.1051/0004-6361/201321109](https://doi.org/10.1051/0004-6361/201321109)
- Villanova, S., Carraro, G., Geisler, D., Monaco, L., & Assmann, P. 2018, *ApJ*, 867, 34, doi: [10.3847/1538-4357/aae4e5](https://doi.org/10.3847/1538-4357/aae4e5)
- Wegg, C., Gerhard, O., & Portail, M. 2015, *MNRAS*, 450, 4050, doi: [10.1093/mnras/stv745](https://doi.org/10.1093/mnras/stv745)
- Weisz, D. R., Dolphin, A. E., Skillman, E. D., et al. 2013, *MNRAS*, 431, 364, doi: [10.1093/mnras/stt165](https://doi.org/10.1093/mnras/stt165)
- Wielgórski, P., Pietrzyński, G., Gieren, W., et al. 2017, *ApJ*, 842, 116, doi: [10.3847/1538-4357/aa7565](https://doi.org/10.3847/1538-4357/aa7565)
- Yuan, W., Riess, A. G., Macri, L. M., Casertano, S., & Scolnic, D. M. 2019, *ApJ*, 886, 61, doi: [10.3847/1538-4357/ab4bc9](https://doi.org/10.3847/1538-4357/ab4bc9)